Computational Studies of Electron Paramagnetic Resonance Parameters for Paramagnetic Molybdenum Complexes. 1. Method Validation on Small and Medium-Sized Systems

Jörg Fritscher,*,† Peter Hrobárik,‡ and Martin Kaupp*,§

Institute of Physical and Theoretical Chemistry, J. W. Goethe University of Frankfurt, and Center for Biological Magnetic Resonance, Max-von-Laue-Straβe 7, D-60438 Frankfurt, Germany, Institute of Inorganic Chemistry, Slovak Academy of Sciences, Dúbravská cesta 9, SK-84536 Bratislava, Slovakia, and Institut für Anorganische Chemie, Universität Würzburg, Am Hubland, D-97074 Würzburg, Germany

Received: January 25, 2007

A variety of density functional methods have been evaluated in the computation of electronic *g*-tensors and molybdenum hyperfine couplings for systems ranging from the Mo atom through $Mo^{III}N$, $[Mo^{V}OCl_4]^-$, and $[Mo^{V}OF_5]^{2-}$ to two larger Mo^{V} complexes $MoXLCl_2$ (X = O, S; L = tris(3,5-dimethylpyrazolyl)hydroborate anion). In particular, the influence of the molybdenum basis set and of various exchange−correlation functionals with variable admixtures of Hartree−Fock exchange on the computed EPR parameters have been evaluated in detail. Careful basis-set studies have provided a moderate-sized 12s6p5d all-electron basis on molybdenum that gives hyperfine tensors in excellent agreement with much larger basis sets and that will be useful for calculations on larger systems. The best agreement with experimental data for both hyperfine and *g*-tensors is obtained with hybrid functionals containing approximately 30−40% Hartree−Fock exchange. Only for $MoSLCl_2$ does increasing spin contamination with increasing exact-exchange admixture restrict the achievable computational accuracy. In all cases, spin−orbit corrections to the hyperfine tensors are sizable and have to be included in accurate calculations. Scalar relativistic effects enhance the isotropic Mo hyperfine coupling by approximately 15−20%. Two-component *g*-tensor calculations with variational inclusion of spin−orbit coupling show that the $\Delta g_{||}$ components in $[Mo^{V}OCl_4]^-$ and $[Mo^{V}OF_5]^{2-}$ depend on higher-order spin−orbit contributions and are thus described insufficiently by the usual second-order perturbation approaches. Computed orientations of *g*- and hyperfine tensors relative to each other and to the molecular framework for the $MoXLCl_2$ complexes provide good agreement between theory and single-crystal electron paramagnetic resonance experiments. In these cases, the hyperfine tensor orientations are influenced only slightly by spin−orbit effects.

1. Introduction

A number of molybdenum-containing enzymes, such as, for example, sulfite oxidase, nitrate reductase, xanthine oxidase, xanthine dehydrogenase, dimethylsulfoxide (DMSO) reductase, or polysulfide reductase, play an important role in biological two-electron redox processes.[1−4] Since these catalytic reactions directly involve the molybdenum ion, it is of great importance for a deeper understanding of the reaction mechanism to study the structure of the catalytically active molybdenum binding site.[4] Due to the occurrence of paramagnetic Mo^{V} species during the catalytic cycles of all of these enzymes, electron paramagnetic resonance (EPR) spectroscopy[5] can be a valuable tool to reveal details about the molybdenum coordination sphere.[1,4,6−9]

The parameters that can be extracted from EPR spectra, such as electronic *g*-tensors, hyperfine coupling (HFC) tensors, or nuclear quadrupole coupling (NQC) tensors, contain indirect information about the electronic and molecular structure of the metal binding site.[5,6,10−14] However, it is often difficult or even impossible to relate these spin Hamiltonian EPR parameters to structural information.[13,15] It may even be hard to find a unique solution for the simulation of the EPR spectra using the spin Hamiltonian concept. Thus, models or theories are needed that are able to provide the link between molecular structure and EPR parameters. In some specific cases, ligand-field theory, semiempirical McConnell relations, or the point-dipole approximation are suitable for the interpretation of EPR parameters.[5,10,12,14,16,17] In general, these approaches fail for systems that possess a complicated electronic structure or that are not yet calibrated for the use of semiempirical theories.[15] It is here that explicit quantum chemical calculations come into play and are very useful for correlating experimental EPR data with molecular structure.[13,15,18,19] Due to the sizes of the systems that have to be considered to describe the local magnetic properties of metal binding sites, density functional theory (DFT)[20] is the method of choice. It provides the best compromise between accuracy of the theoretical level and computation time, thus providing a very useful basis for the calculation of *g*- and HFC tensors.[18,21−30]

While substantial validation work during the past 5−10 years has established the scope and accuracy of DFT methods for calculating EPR parameters for 3d-complexes,[24−26,28−34] much less is known for 4d systems. This holds particularly for the hyperfine tensors. Before treating the molybdenum binding sites of real biological systems and drawing extensive conclusions about their structure based on computational results, a critical validation of the available DFT methods and basis sets for

* Authors to whom correspondence should be addressed. E-mail: j.fritscher@epr.uni-frankfurt.de; kaupp@mail.uni-wuerzburg.de.
† J. W. Goethe University of Frankfurt and Center for Biological Magnetic Resonance.
‡ Slovak Academy of Sciences.
§ J. Maximilians University of Würzburg.

10.1021/jp070638y CCC: $37.00
Published on Web 04/05/2007

treating systems containing the 4d transition metal molybdenum is thus necessary to avoid misinterpretation.

Until now only a few computational studies of *g*- and molybdenum HFC tensors of Mo^V compounds have been performed. Early studies in this field employed the bonding coefficients of self-consistent-field (SCF)-MS-Xα wave functions in approximate linear combination of atomic orbital (LCAO) expressions for the *g*- and HFC tensors.[35] In other work, single-excitation configuration interaction (SCI) wave functions at the intermediate neglect of differential overlap (INDO/S) level have been used in second-order perturbation expressions for the *g*-tensor.[36] Furthermore, simple connections from DFT to ligand-field-theory perturbation expressions for *g*- and HFC values[37] or the INDO-CI-Stone method for the computation of principal *g*-values[38] have been employed.

More recent studies of *g*- and HFC tensors of transition metal complexes have shown that modern DFT provides a useful basis for the calculation of both properties.[13,18,24,27−29,31,33,34,39−42] Patchkovskii and Ziegler reported the first systematic study on the prediction of *g*-tensors for some axial d^1 $[MEX_4]^{z-}$ systems (M = V, Cr, Mo, W, Tc, Re; E = N, O; X = F, Cl, Br) using DFT with local density approximation (LDA) and gradient-corrected approximation (GGA) functionals.[34] While that study suggested a relatively small dependence of the results on the exchange−correlation functional, experience for 3d-complexes has indicated that the admixture of exact exchange in hybrid functionals increases the *g*-shifts and thereby improves agreement with experiment in typical systems with metal-centered spin density.[26,28] (The opposite behavior was found for ligand-centered radicals.[39,43]) Moreover, LDA and GGA functionals underestimate core−shell spin polarization at the metal center, which is important for the calculation of metal hyperfine coupling constants (HFCCs).[29,30] It has been shown that hybrid functionals may enhance the core−shell spin polarization and thus often yield better isotropic metal HFCCs. However, increased admixture of Hartree−Fock exchange may be coupled to spin contamination in unrestricted treatments, which under certain circumstances deteriorates computed hyperfine coupling tensors and *g*-tensors, especially when the singly occupied molecular orbitals (SOMOs) are significantly metal−ligand antibonding.[30] Recent work based on so-called localized hybrid potentials did not eliminate the spin-contamination problem per se but provided *g*-tensors that were not affected negatively by it.[44,45]

Turning to molybdenum systems in particular, only a few EPR property calculations have been performed besides the pioneering work of Patchkovskii and Ziegler.[34] Two further LDA/GGA DFT studies by Patchkovskii and Ziegler—one on *g*-tensors of d^1 metal porphyrins[24] and a benchmark study on the calculation of *g*-tensors of high-spin radicals[46] (e.g., MoN)—and a few general methodological *g*-tensor validation studies including some paramagnetic molybdenum species are available,[27,28,47] including one study using hybrid functionals.[28] During the course of the present work, two other studies treated the *g*- and molybdenum HFC tensors[41] and ligand HFC and ^{17}O NQC values,[48] respectively, of two larger Mo^V complexes with state-of-the-art computational methods (INDO/S configuration interaction calculations and/or one-component DFT calculations). However, systematic validation studies of exchange−correlation functionals and basis sets (for HFC calculations) and of the spin-contamination problem for paramagnetic molybdenum systems have not been performed. In this paper and in a companion paper[49] we evaluate thus in detail the unrestricted Kohn−Sham methods implemented[28,32,50] in our MAG-ReSpect program system[51] to compute electronic *g*-tensors and molybdenum HFC tensors for a large variety of paramagnetic Mo systems. In the present work, the test systems range from the Mo atom via the MoN diatomic molecule through the small Mo^V complexes $[MoOCl_4]^-$ and $[MoOF_5]^{2-}$ to the larger and less symmetrical Mo^V systems $MoXLCl_2$ (X = O, S; L = tris(3,5-dimethylpyrazolyl)hydroborate anion, also frequently abbreviated as Tp* in the literature) (Figure 1). The computational results are compared with experimental data, including tensor orientations from single-crystal experiments for the less symmetrical $MoXLCl_2$ systems. In the second paper[49] we will provide analyses of EPR parameters for a larger series of more complicated Mo^V complexes that are even closer models for the Mo^V coordination in molybdopterin enzymes.

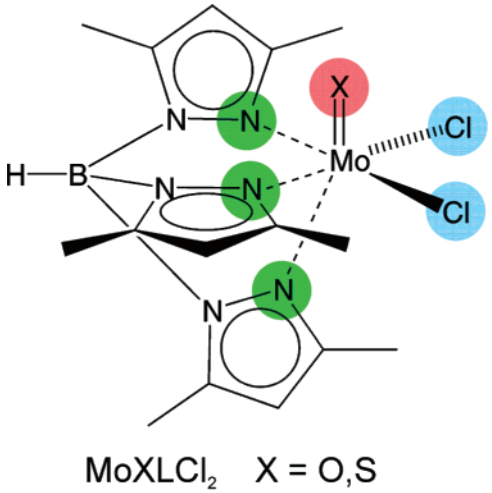

Figure 1. Schematic structure of the two larger Mo^V complexes studied in this work ($MoOLCl_2$ and $MoSLCl_2$ with L = tris(3,5-dimethylpyrazolyl)hydroborate).

2. Theoretical Formalism and Computational Details

The theoretical background of EPR spin Hamiltonian parameters and their computation is covered in detail in the literature;[10,18,52−54] hence only the most relevant points will be summarized here.

***g*-Tensor Calculations.** The *g*-tensor **g** will be provided as correction Δ**g** to the free electron *g*-value g_e (in this work the *g*-shift tensor Δ**g** will be given in ppm, i.e., in units of 10^{-6})

$$\mathbf{g} = g_e\mathbf{1} + \Delta\mathbf{g}$$

with $g_e = 2.002319$. Up to the level of second-order perturbation theory using the Breit−Pauli Hamiltonian, the *g*-shift Δ**g** consists of three terms[53,55]

$$\Delta\mathbf{g} = \Delta\mathbf{g}^{SO/OZ} + \Delta\mathbf{g}^{RMC} + \Delta\mathbf{g}^{GC}$$

of which the "paramagnetic" second-order spin−orbit/orbital Zeeman cross term $\Delta\mathbf{g}^{SO/OZ}$ dominates (except for extremely small Δ*g*-values).[53] Within our unrestricted coupled−perturbed Kohn−Sham approach using hybrid density functionals, its Cartesian components *ij* are computed (in atomic units) as[28]

$$\Delta g_{ij}^{SO/OZ} = \frac{\alpha^2}{2} g_e \left[\sum_k^{occ(\alpha)} \sum_a^{virt(\alpha)} \frac{\langle \psi_k^\alpha | \mathbf{h}_j^{SO} | \psi_a^\alpha \rangle \langle \psi_a^\alpha | F_i' | \psi_k^\alpha \rangle}{\epsilon_k^\alpha - \epsilon_a^\alpha} - \sum_k^{occ(\beta)} \sum_a^{virt(\beta)} \frac{\langle \psi_k^\beta | \mathbf{h}_j^{SO} | \psi_a^\beta \rangle \langle \psi_a^\beta | F_i' | \psi_k^\beta \rangle}{\epsilon_k^\beta - \epsilon_a^\beta} \right] \quad (1)$$

where α is the fine-structure constant, $\mathbf{h}_i^{SO}$ is explained below, F_i' is the perturbed Fock operator, with $F_i' = \hat{\ell}_{O,i} - (2/\alpha)a_0 \sum_{k=1}^{n/2} K_{k,i}'$, where $\hat{\ell}_{O,i}$ is a spatial component of the orbital Zeeman operator, $K_{k,i}'$ is the response-exchange operator, and a_0 is the weight of Hartree−Fock exchange depending on the specific hybrid functional used. ψ_i^σ and ϵ_i^σ are spin-polarized Kohn−Sham orbitals and orbital energies, respectively. LDA and/or GGA functionals lead to an uncoupled (UDFT) treatment for this second-order term ($a_0 = 0$). The relativistic mass correction term $\Delta\mathbf{g}^{RMC}$ and the one-electron part of the gauge correction term $\Delta\mathbf{g}^{GC}$ are also included in our approach.[27,28]

To evaluate the importance of spin−orbit contributions to the *g*-tensor beyond leading order in perturbation theory, we have carried out calculations on two complexes ($[MoOCl_4]^-$ and $[MoOF_5]^{2-}$) using a recently implemented relativistic two-component Douglas−Kroll−Hess approach.[56] This *g*-tensor implementation is the first method that includes spin−orbit coupling variationally in a relativistic framework but also recovers spin polarization faithfully. It requires three two-component non-collinear spin-density functional calculations with orthogonal directions of total magnetization.

Hyperfine Coupling Tensor Calculations. Using the Breit−Pauli Hamiltonian[53,55] and a vector potential corresponding to a pointlike magnetic dipole moment of nucleus *N*, the isotropic hyperfine coupling constant $A_{iso}'(N)$ is at first order approximated by the Fermi contact term $A_{FC}(N) = A_{iso}(N)$, which can be written as[50,53]

$$A_{iso}(N) = A_{FC}(N) = \frac{4\pi}{3}\alpha^2 g_e \gamma_N \frac{1}{2}\langle S_Z\rangle^{-1} \sum_{\mu,\nu} P_{\mu\nu}^{\alpha-\beta}\langle\varphi_\mu|\delta(\mathbf{R}_N)|\varphi_\nu\rangle \quad (2)$$

Here γ_N is the gyromagnetic ratio of nucleus *N*, g_e is the free electron *g*-value, $\langle S_Z\rangle$ is the expectation value of the *z*-component of the total electronic spin, and $P_{\mu\nu}^{\alpha-\beta}$ is the $\mu\nu$ element of the spin-density matrix in the atomic orbital basis $\{\varphi_\mu\}$. The Cartesian components T_{ij} of the anisotropic dipolar tensor **T** are given by[50,53]

$$T_{ij}(N) = \frac{1}{2}\alpha^2 g_e \gamma_N \frac{1}{2}\langle S_Z\rangle^{-1} \sum_{\mu,\nu} P_{\mu\nu}^{\alpha-\beta}\langle\varphi_\mu|\mathbf{r}_N^{-5}(\mathbf{r}_N^2\delta_{ij} - 3r_{N,i}r_{N,j})|\varphi_\nu\rangle \quad (3)$$

where $\mathbf{r}_N = \mathbf{r} - \mathbf{R}_N$ ($\mathbf{R}_N$ is the position vector of nucleus *N*). $A_{FC} = A_{iso}$ and T_{ij} contribute to the nonrelativistic part of the HFC tensor

$$A_{ij}(N) = T_{ij}(N) + \delta_{ij}A_{iso}(N)$$

The dominant spin−orbit (SO) correction term to the HFC tensor arises as a second-order cross term between the one- and two-electron SO Hamiltonian $\mathbf{h}_i^{SO}$ and the perturbed Fock operator $F_{N,j}'$[32,50]

$$A_{ij}^{SO-I(1)}(N) + A_{ij}^{SO-I(2)}(N) = \frac{1}{2}\alpha^4 g_e \gamma_N \frac{1}{2}\langle S_Z\rangle^{-1}\left[\sum_k^{occ(\alpha)}\sum_a^{virt(\alpha)} \frac{\langle\psi_k^\alpha|\mathbf{h}_i^{SO}|\psi_a^\alpha\rangle\langle\psi_a^\alpha|F_{N,j}'|\psi_k^\alpha\rangle}{\epsilon_k^\alpha - \epsilon_a^\alpha} - \sum_k^{occ(\beta)}\sum_a^{virt(\beta)} \frac{\langle\psi_k^\beta|\mathbf{h}_i^{SO}|\psi_a^\beta\rangle\langle\psi a^\beta|F_{N,j}'|\psi_k^\beta\rangle}{\epsilon_k^\beta - \epsilon_a^\beta}\right] \quad (4)$$

with $F_{N,j}' = (\hat{\ell}_{N,j}/r_N^3) - (2/\alpha)a_0 \sum_{k=1}^{n/2} K_{k,j}'$, where $(\hat{\ell}_{N,j}/r_N^3)$ is the paramagnetic nuclear-spin electron-orbit operator and $K_{k,j}'$ is the response-exchange operator.

For better comparison with experimental values the SO correction A_{ii}^{SO} to the principal components A_{ii} of the nonrelativistic HFC tensor **A** are given in terms of an isotropic pseudocontact (A_{PC}) and anisotropic ($T_{ii,orb}$) term

$$A_{ii}^{SO}(N) = A_{PC}(N) + T_{ii,orb}(N)$$

Taking these definitions, the components of the complete HFC tensor **A′** (up to second-order perturbation theory) can be written as

$$A_{ij}'(N) = T_{ij}(N) + T_{ij,orb}(N) + \delta_{ij}(A_{FC}(N) + A_{PC}(N)) = T_{ij}'(N) + \delta_{ij}A_{iso}'(N)$$

and in the case of axial symmetry

$$T_{dip} = T_{11} = T_{22} = -T_{33}/2 = T_\perp = -T_{||}/2$$

$$T_{orb} = T_{11,orb} = T_{22,orb} = -T_{33,orb}/2 = T_{\perp,orb} = -T_{||,orb}/2$$

and

$$T_{dip}' = T_{dip} + T_{orb}$$

and the principal components of **A′** can be expressed using only two parameters

$$A_\perp'(N) = A_{11}'(N) = A_{22}'(N) = T_{dip}' + A_{iso}' \quad \text{and} \quad A_{||}'(N) = A_{33}'(N) = -2T_{dip}' + A_{iso}'$$

The quantities A_{iso}' and T_{ii}' (including SO corrections) represent the best description of the experimental EPR parameters and should therefore be used for comparison with experimental data. In the following, we will generally refer to the molybdenum hyperfine interaction and the argument *N* will be omitted. Furthermore, the T_{ii}, $T_{ii,orb}$, and T_{ii}' values will always be given as eigenvalues of the corresponding tensors, i.e., in their own principal axis systems. The sum relation $T_{ii}' = T_{ii} + T_{ii,orb}$ will only be fully valid if the principal axis systems of all three tensors coincide. Since this is not the case for less symmetrical compounds, T_{ii}' will in general deviate from the sum of the two eigenvalues T_{ii} and $T_{ii,orb}$. The magnitude of this deviation is an indicator of how much the axis systems differ from each other.

Calculation of EPR Parameters. Practically, the one-component *g*- and HFC tensor calculations were carried out in two steps: First the unrestricted Kohn−Sham orbitals were generated with the Gaussian 03 program[57] and were transferred to the MAG-ReSpect property package[51] by suitable interface routines. The converted orbitals were then used to carry out the *g*-tensor and HFC tensor calculations. In the Gaussian 03 single-point SCF calculations tight SCF convergence criteria (energy and density matrix convergence 10^{-6} and 10^{-8} a.u., respectively) and an ultrafine integration grid (99 radial shells and 590 angular points per shell) were used. The two-component *g*-tensor calculations on $[MoOCl_4]^-$ and $[MoOF_5]^{2-}$ were done with a recent two-component version[56] of ReSpect and MAG-ReSpect. A FINER angular integration grid with 64 radial shells (this corresponds to ca. 6000 points per atom) was used.

The following exchange−correlation functionals were used and compared: (a) the local density approximation (LDA) with Slater exchange and Vosko−Wilk−Nusair (VWN) correlation[58] (cf. SVWN5 keyword in Gaussian 03); (b) the BP86[59−61] GGA

(generalized gradient approximation) functional; (c) the B3PW91[62−65] hybrid functional, incorporating 20% exact Hartree−Fock (HF) exchange; and (d) user-defined one-parameter BPW91-based hybrid functionals (as available within the Gaussian 03 program) of the general form

$$E_{XC}^{hybrid} = a_0 E_X^{HF} + (1 - a_0) E_X^{B88} + E_C^{PW91}$$

with a_0 indicating the amount of Hartree−Fock exact exchange E_X^{HF} (chosen as 0.30, 0.40, 0.50, 0.60, or 0.70, in the following denoted as BPW91-30HF, BPW91-40HF, etc.).

The property calculations in MAG-ReSpect used the atomic mean-field (AMFI) approximation[66,67] to compute the matrix elements of the spin−orbit operator. A common gauge at the molybdenum nucleus was used for the *g*-tensors. (The *g*-tensor is generally much less gauge-dependent than, for example, NMR chemical shifts.[21])

Since no molybdenum Gaussian-type orbital (GTO) basis sets specifically tailored for the computation of EPR properties were available, one task of this work was the construction of a suitable basis set that is flexible enough but computationally efficient. Therefore, we have investigated the dependence of the EPR parameters of small molybdenum compounds (Mo atom, MoN, $[MoOCl_4]^-$, and $[MoOF_5]^{2-}$) on the choice of the basis set employing various contracted and fully uncontracted basis sets. These basis sets were constructed by fully uncontracting and then partially recontracting (from inside out) the all-electron TZVP basis set for molybdenum from Ahlrichs and May.[68] The contractions were performed in the same way and using the same contraction coefficients as in the original contracted (19s14p9d)/[8s6p5d] {84211111/641111/51111} TZVP basis set. The following basis sets were generated for this study: 19s14p9d (fully uncontracted), 19s14p5d, 19s9p5d, 19s6p5d, 12s9p5d, 12s6p5d, 9s6p5d, and 8s6p5d (fully contracted). To evaluate the influence of f-polarization functions at the metal, we have also carried out some calculations in which the single f-set (exponent 1.04835114) of Weigend (from the Turbomole standard TZVPP basis set) has been added to yield a fully uncontracted 19s14p9d1f basis set. The (19s14p9d)/[12s6p5d] {811111111111/641111/51111} contraction was found to be an optimal compromise between accuracy and computational effort (see Results and Discussion section below). For $[MoOCl_4]^-$ one calculation with a very large and flexible, fully uncontracted 23s19p12d Hirao basis set[69] for molybdenum was performed. Huzinaga−Kutzelnigg-type IGLO-II basis sets[70] were used for all other atoms.

In some calculations on $[MoOCl_4]^-$ and $[MoOF_5]^{2-}$, scalar relativistic effects on molybdenum hyperfine tensors were evaluated using a second-order Douglas−Kroll−Hess (DKH) approach developed in ref 71 and extended recently to a Gaussian charge finite-nucleus model.[72] These calculations employed the fully uncontracted 23s19p12d Hirao basis set[69] for molybdenum combined with fully uncontracted DZVP basis sets[73] for the other atoms. When a finite-nucleus model was employed, this was done consistently for both the nuclear charge in the second-order DKH SCF calculation (in the Gaussian 03 program) and for the nuclear magnetic moment in the HFC calculation[72] (in MAG-ReSpect).

Molecular Structures and Structure Optimizations. The electronic ground states are ^7S for $[Mo^0]$[74] and $^4\Sigma$ for $[Mo^{III}N]$.[74,75] $[Mo^VOCl_4]^-$ and $[Mo^VOF_5]^{2-}$ possess C_{4v} symmetry and a $^2B_2$ ground state.[37] The larger "octahedral" hexacoordinated $[Mo^VXCl_2]$ systems (X = O or S)[76] exhibit doublet ground states with structures close to C_s symmetry (cf. Figure 1). For MoN the experimental Mo−N bond length of 1.636 Å[75] was used. To be able to compare with previous computations,[27,28,34] DFT-optimized coordinates (SVWN results) from Patchkovskii and Ziegler[34] were taken for $[MoOCl_4]^-$. The structures of $[MoXLCl_2]$ were optimized (starting from crystallographic data for related systems) at the unrestricted DFT level (BP86[59−61] functional) with the Turbomole[77] code. For molybdenum an energy-adjusted small-core effective core potential[78] was used together with a TZVP valence basis set (7s6p5d)/[5s3p3d] (default basis in Turbomole for atoms from Rb to Rn). TZVP all-electron basis sets[79] were employed for all other atoms. The Coulomb term was approximated by the resolution of the identity (RI) method[80,81] (density fitting with a standard TZVP auxiliary basis set[80]) to speed up the computations. The same computational level was used to optimize $[MoOF_5]^{2-}$. Cartesian coordinates of the optimized structures are available in the Supporting Information (Tables S3 and S4). Agreement between optimized and experimental structures (where available) was generally good.

3. Results and Discussion

Molybdenum Basis-Set Studies. In view of the above-mentioned lack of well-calibrated molybdenum basis sets for EPR parameter calculations, we used calculations on the Mo atom, the MoN molecule, and the two well-studied[27,28,34,35,37,38,82−84] small Mo^V complexes $[MoOCl_4]^-$ and $[MoOF_5]^{2-}$ to construct a suitable basis set for molybdenum that is accurate but sufficiently efficient computationally to be applied to large systems.

In contrast to the d^1 Mo^V systems, where the unpaired electron is almost completely located in a metal d-orbital, one of the singly occupied atomic orbitals of the Mo atomic ground state is the 5s-orbital, and one of the singly occupied molecular orbitals (SOMOs) of MoN is a σ-orbital. There is thus a direct SOMO contribution to the Fermi contact interaction for Mo and MoN, and spin-polarization effects[30,85] play a minor role for A_{iso} in these species. Figure 2 shows the dependencies of the hyperfine couplings on the metal basis set (the less dramatic dependence of the *g*-values is shown in Figures S1 and S2 in the Supporting Information), using the B3PW91 hybrid functional. The isotropic hyperfine couplings exhibit only little change upon recontraction of the 19s14p9d basis down to 12s6p5d. But any further contraction of the s-functions leads to an appreciable deviation (e.g., of approximately 17 MHz for Mo) from the fully uncontracted basis-set result. T_{dip} in MoN (Figure 2b) and the *g*-tensor components in Mo and MoN (Figure S2) are almost invariant toward basis-set contraction. Addition of an f-function has a nonnegligible effect on A_{iso} in MoN (Figure 2b) and changes $\Delta g_\perp$ by approximately 10% (from ca. −6400 to ca. −7100 ppm; Figure S2). The latter change is approximately the order of magnitude of the usual experimental errors for many EPR signals of molybdenum compounds. The use of metal f-functions is thus not crucial in *g*-tensor calculations. These results show clearly that the *g*-values and dipolar hyperfine tensors exhibit only little dependence on the basis set. However, a sufficiently flexible s-function basis set in the outer-core part is essential for accurate isotropic metal hyperfine couplings. This is similar to the results obtained for 3d-complexes.[29] The smallest basis set that yields only small deviations from the "basis-set limit" accuracy (assumed here for the fully uncontracted TZVP basis set) is the 12s6p5d basis set.

Table 1 provides a corresponding basis-set study for *g*- and HFC tensors of $[MoOCl_4]^-$ and $[MoOF_5]^{2-}$ (Figure 3 illustrates

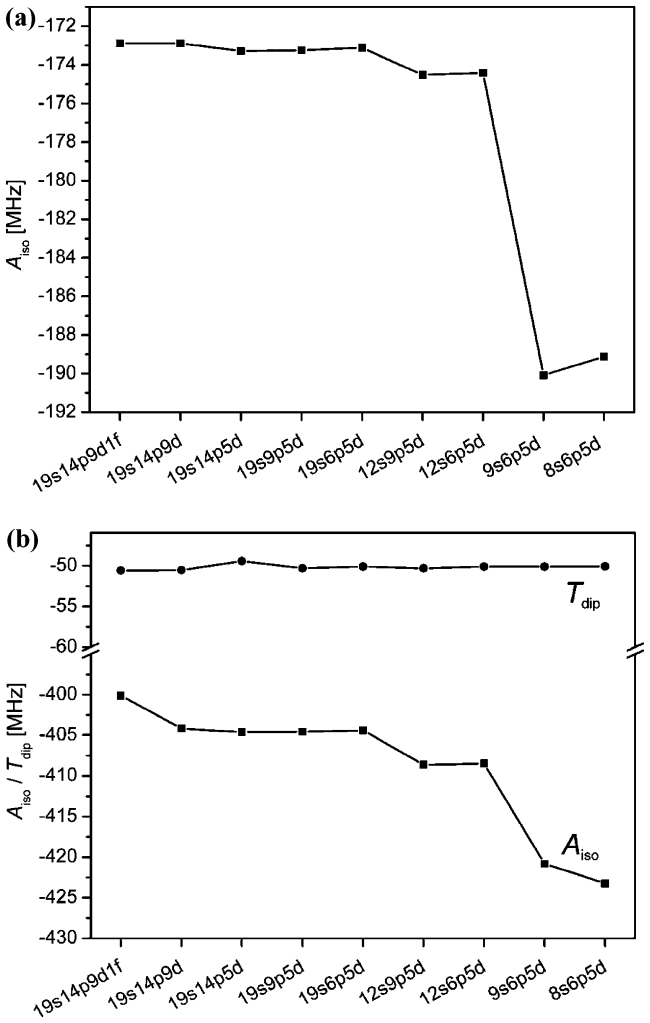

Figure 2. Dependence of ^{95}Mo A_{iso} (squares) and T_{dip} (circles) on the size of the molybdenum basis set for (a) the Mo^0 (^7S) atom and (b) the MoN ($^4\Sigma$) molecule. The calculations were performed using the B3PW91 density functional and the IGLO-II basis set for nitrogen.

results for the former complex). The $\Delta g_\perp$- and $\Delta g_{||}$-shifts of $[MoOCl_4]^-$ exhibit a considerable change upon addition of a metal f-function, and the dependence on the contraction of the metal d-functions is also clearly notable. But again, both effects are not far outside the usual experimental error margins of *g*-tensor evaluations and much smaller than influences of different density functionals. All further basis-set contractions do not influence the *g*-shift parameters. As was already found for MoN, T_{dip} exhibits negligible basis-set dependence, whereas A_{iso} is reduced substantially (by about 28 MHz) when the s-functions are contracted from 12s to 9s (Figure 3 and Table 1). The basis-set dependence of the EPR parameters of $[MoOF_5]^{2-}$ is very similar (Table 1). For $[MoOCl_4]^-$ we applied also a still larger, fully uncontracted 23s19p12d basis set of Hirao (Table 1). Differences relative to the fully uncontracted TZVP basis are minor, except for a somewhat larger A_{iso}. Here the influence of the tighter s-functions in the Hirao basis set comes into play.

We have also investigated potential limitations of our 12s6p5d molybdenum basis set that could be due to the lack of very diffuse p- or d-functions. For this purpose we have added a more diffuse p-function (exponent, 0.0300) and/or a more diffuse d-function (exponent, 0.0596) to the 12s6p5d basis. (Exponents were obtained by dividing those of the most diffuse p- or d-functions already present by a factor of 3.) BP86 calculations for $[MoOCl_4]^-$ employing the extended basis sets 12s7p5d, 12s6p6d, and 12s7p6d for molybdenum provided generally effects of less than 1 MHz for HFCs and of less than 1 ppt for *g*-tensor components.

We have thus identified the 12s6p5d basis as the smallest basis set that still yields EPR parameters close to the "basis-set limit" values. It appears therefore suitable as a standard molybdenum basis set for EPR parameter calculations on larger systems.

Dependence on Exchange−Correlation Functional: $[MoOCl_4]^-$ and $[MoOF_5]^{2-}$. The second task of this work was to find generally applicable exchange−correlation functionals that provide accurate EPR parameters for Mo^V complexes. The initial calculations were performed for the small C_{4v} symmetrical model complexes $[MoOCl_4]^-$ and $[MoOF_5]^{2-}$ (Table 2 and Figure 4). Starting with the *g*-tensors, we note that for a C_{4v} d^1 system like $[MoOCl_4]^-$ with a d_{xy} SOMO the dominant contributions to $\Delta g_\perp$ arise from couplings of the SOMO to d_{xz}- and d_{yz}-based MOs and $\Delta g_{||}$ is dominated by coupling from the SOMO to a $d_{x^2-y^2}$-based MO (as has been discussed previously[34,37]). Closer analysis (cf. discussion in the Supporting Information as well as Table S1 and Figure S3 for detailed MO analyses of our *g*-tensor calculations) indicates also some (positive) contributions from couplings of doubly occupied MOs of Mo−Cl bonding character to the β-component of the SOMO. In the course of the analyses it has become obvious that non-ligand-field transitions have to be considered to explain the observed *g*-shifts and that metal−ligand covalency and ligand SO coupling plays a nonnegligible role. These aspects have already been noted in earlier works,[34,36,37,82,86] and it has now become possible to put the whole discussion on a firmer quantitative basis.

The $g_{||}$-component is furthermore influenced by higher-order spin−orbit contributions (see below). Table 2 and Figure 4 show that the negative perpendicular *g*-shift component for $[MoOCl_4]^-$ reaches the experimental value at an exact-exchange admixture of approximately 30−40%. In contrast, B3PW91 overshoots already slightly for $[MoOF_5]^{2-}$. Given the potential environmental effects on these ions, this does not allow a "best functional" to be chosen. Even at 70% HF exchange admixture, the negative $\Delta g_{||}$-values are not yet reached. This points to a systematic error of the one-component second-order perturbation approach used that we will address below in two-component calculations. We will refrain here from extensively comparing our results for these two complexes in detail with previous calculations, which range from INDO-CI results[38] via early, crude DFT calculations[37] to state-of-the-art DFT results with GGA functionals[27,28,34] and a few hybrid DFT data.[28] The reason for this is that the semiempirical results are considered too approximate and unreliable quantitatively and that GGA functionals in DFT are not considered very appropriate either. Some of the spin−orbit operators used previously were also far from the current state of the art. We prefer to analyze the influence of various parameters by comparing different functionals in one implementation and with the same basis sets. Swann and Westmoreland[37] have used a strongly simplified DFT implementation together with one-electron SO coupling parameters from experimental data, and Patchkovskii and Ziegler[34] employed LDA and GGA functionals in combination with effective potentials for the SO operator. Both theoretical models are not able to reproduce the negative parallel *g*-shifts and yield perpendicular *g*-shifts that are still not negative enough for $[MoOCl_4]^-$. Our present one-component results agree qualitatively with the more recent calculations[28,34] and furthermore reveal that the use of hybrid functionals leads to a correct

TABLE 1: Dependence of Hyperfine Coupling and *g*-Tensor Principal Values (without SO-HFC Corrections) on the Size of the Molybdenum Basis Set for $[MoOCl_4]^-$ ($^2B_2$) and $[MoOF_5]^{2-}$ ($^2B_2$)[a]

complex	basis set	$g_{\|\|}$	$g_\perp$	$\Delta g_{\|\|}$	$\Delta g_\perp$	A_{iso}	T_{dip}	$\langle S^2\rangle$
$[MoOCl_4]^-$	23s19p12d (Hirao fully uncontracted)	1.9972	1.9504	−5125	−51884	85.6	−34.8	0.7576
	19s14p9d1f (fully uncontracted)	1.9979	1.9506	−4420	−51720	89.2	−34.7	0.7572
	19s14p9d (fully uncontracted)	1.9993	1.9502	−3044	−52084	87.8	−34.6	0.7575
	19s14p5d	2.0000	1.9511	−2289	−51188	87.1	−34.0	0.7575
	19s9p5d	2.0000	1.9510	−2333	−51271	87.2	−34.6	0.7575
	19s6p5d	1.9999	1.9510	−2419	−51351	86.1	−34.3	0.7561
	12s9p5d	2.0000	1.9510	−2327	−51271	89.9	−34.6	0.7575
	12s6p5d	2.0000	1.9510	−2320	−51320	90.1	−34.3	0.7575
	9s6p5d	2.0000	1.9510	−2339	−51320	62.7	−34.3	0.7575
	8s6p5d	2.0000	1.9510	−2339	−51320	72.8	−34.3	0.7575
	exp.[83]	1.9650	1.9468	−37320	−55520	144.6	−41.4	
$[MoOF_5]^{2-}$	19s14p9d1f (fully uncontracted)	1.9217	1.9050	−80586	−97278	112.6	−38.2	0.7578
	19s14p9d (fully uncontracted)	1.9222	1.9028	−80144	−99550	111.3	−38.0	0.7581
	12s6p5d	1.9238	1.9040	−78495	−98291	114.1	−37.7	0.7581
	9s6p5d	1.9238	1.9041	−78495	−98235	83.4	−37.7	0.7581
	exp.[84]	1.874	1.911	−128320	−91320	183.1	−47.8	

[a] All computations were performed using the B3PW91 density functional and IGLO-II basis sets for all atoms except molybdenum. All HFC constants are given in MHz, and *g*-shifts (Δg) are given in ppm.

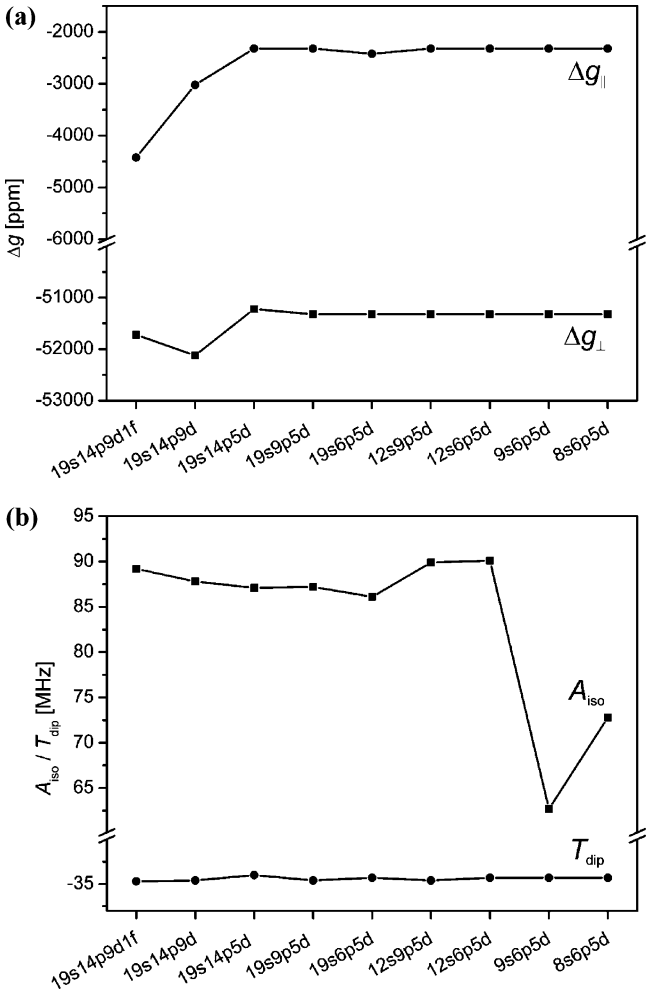

Figure 3. Dependence of (a) $\Delta g_\perp$ (squares) and $\Delta g_{||}$ (circles) and (b) ^{95}Mo A_{iso} (squares) and T_{dip} (circles) on the size of the molybdenum basis set for $[MoOCl_4]^-$ ($^2B_2$). The calculations were performed using the B3PW91 density functional and IGLO-II basis sets for all other atoms.

prediction of the negative sign of the parallel *g*-shift. Therefore, our hybrid DFT calculations for $[MoOCl_4]^-$ yield *g*-shifts in better agreement with experimental data than the previous calculations. We note, however, that our present results for $[MoOCl_4]^-$ are lower than the results with the corresponding functionals from ref 28 by approximately 15−20 ppt for $\Delta g_\perp$ and by 6−16 ppt for $\Delta g_{||}$. Closer analyses (data not shown) indicate that these differences are due to an insufficiently flexible Mo d-basis set in ref 28. (This problem does not affect the bulk of the calculations in that work, which was focused on 3d-complexes.)

Turning to the ^{95}Mo HFC tensors, it appears at first sight that larger HF exchange admixtures are required to approach the experimental values (we focus on the A'_{iso} and T'_{dip} values obtained after inclusion of spin−orbit corrections, cf. discussion below) for both isotropic and anisotropic contributions. However, already around 40% HF exchange, where good *g*-tensors may be obtained, the agreement with experimental hyperfine tensors is acceptable. Moreover, we will show below that, in contrast to the HFC anisotropy, A_{iso} is increased on the order of ca. 15−20% by scalar relativistic effects, which were neglected in the calculations presented in Tables 1 and 2. This suggests again hybrid functionals with approximately 30−40% HF exchange as the preferred choice.

Notably, spin contamination of the Kohn−Sham determinant is small even up to 70% HF exchange admixture (cf. S^2 expectation values), as indicated also by a small and monotonous dependence of the T_{dip} contributions on the functional.[29] This is consistent[30] with an essentially nonbonding character of the d_{xy}-type SOMO in these two complexes. GGA and LDA functionals provide too covalent M−L bonds.[34,87,88] This gives too little spin density on the metal and thus too small *g*-anisotropies,[34] and HF exchange admixture helps by rendering the metal−ligand bond somewhat more ionic.[26,28] Core−shell spin polarization is important for the isotropic hyperfine couplings and is also underestimated by GGA and LDA functionals.[29,30] More detailed studies of the core−shell spin-polarization mechanisms in Mo ions will be reported elsewhere.

Spin−orbit contributions to T'_{dip} are on the order of approximately 7−12% (the fraction increases with more exact-exchange admixture) and render the overall values somewhat more negative (Table 2 and Figure 4b). Contributions to A'_{iso} are close to 15% and increase the positive values further toward experiment. (Due to the negative nuclear *g*-factor of ^{95}Mo, this corresponds to negative spin densities at the nucleus.) It is clear that accurate calculations of the HFC parameters should take the SO contributions into account. A similar magnitude of SO contributions has been found for Cu^{II} $3d^9$ complexes.[25,32] The

TABLE 2: Dependence of Hyperfine Coupling and *g*-Tensor Principal Values (with and without SO-HFC Corrections) on the Choice of the Density Functional for $[MoOCl_4]^-$ ($^2B_2$) and $[MoOF_5]^{2-}$ ($^2B_2$)[a]

complex	functional	$g_{\|\|}$[b]	$g_\perp$[b]	$\Delta g_{\|\|}$[b]	$\Delta g_\perp$[b]	A_{FC} (A_{iso})	A'_{iso}[c]	T_{dip}	T'_{dip}[c]	$\langle S^2\rangle$
$[MoOCl_4]^-$	SVWN5	2.0085	1.9514	6177	−50911	58.9	73.3	−32.5	−34.3	0.7532
	BP86	2.0081 (1.9973)	1.9562 (1.9519)	5822 (−4974)	−46168 (−50364)	72.1	85.7	−32.1	−33.9	0.7540
	B3PW91	2.0000 (1.9888)	1.9510 (1.9464)	−2319 (−13530)	−51319 (−55947)	90.1	105.3	−34.3	−36.6	0.7575
	BPW91-30HF	1.9950 (1.9838)	1.9487 (1.9439)	−7294 (−18537)	−53648 (−58388)	101.3	117.1	−35.2	−37.7	0.7605
	BPW91-40HF	1.9894 (1.9779)	1.9454 (1.9407)	−12907 (−24382)	−56928 (−61665)	110.3	127.0	−36.1	−38.9	0.7641
	BPW91-50HF	1.9833	1.9415	−19005	−60789	119.5	137.2	−37.0	−40.0	0.7691
	BPW91-60HF	1.9768	1.9369	−25521	−65466	128.9	147.6	−37.9	−41.2	0.7764
	BPW91-70HF	1.9699	1.9310	−32408	−71315	138.6	158.4	−38.8	−42.5	0.7872
	exp.[83]	1.9650	1.9468	−37320	−55520	144.6		−41.4		
$[MoOF_5]^{2-}$	SVWN5	1.9332	1.8867	−69083	−115607	75.8	101.6	−36.8	−38.9	0.7534
	BP86	1.9394 (1.9206)	1.9062 (1.9041)	−62933 (−81725)	−96148 (−98225)	95.0	117.9	−36.1	−38.7	0.7543
	B3PW91	1.9238 (1.9030)	1.9040 (1.9021)	−78494 (−99285)	−98290 (−100231)	114.1	138.5	−37.7	−41.2	0.7581
	BPW91-30HF	1.9167 (1.8960)	1.9039 (1.9020)	−85601 (−106354)	−98405 (−100342)	126.5	151.5	−38.1	−42.1	0.7618
	BPW91-40HF	1.9083 (1.8877)	1.9020 (1.8999)	−94071 (−114650)	−100341 (−102447)	136.2	162.0	−38.5	−43.0	0.7666
	BPW91-50HF	1.8994	1.8995	−102919	−102850	146.2	172.8	−38.8	−44.0	0.7739
	BPW91-60HF	1.8901	1.8963	−112193	−106066	156.5	184.2	−39.0	−44.8	0.7850
	exp.[84]	1.874	1.911	−128320	−91320	183.1		−47.8		

[a] All computations were performed using the 12s6p5d basis set for molybdenum and IGLO-II basis sets for all other atoms. All HFC constants are given in MHz, and *g*-shifts (Δg) are given in ppm. [b] One-component *g*-tensor results with relativistic two-component DKH results in parentheses, cf. text. [c] $A'_{iso} = A_{FC} + A_{PC}$ and $T'_{dip} = T_{dip} + T_{orb}$.

SO corrections are slightly more important for $[MoOF_5]^{2-}$ than for $[MoOCl_4]^-$.

It should be noted that the optimized structures used here (and in previous calculations) for the free $[MoOCl_4]^-$ and $[MoOF_5]^{2-}$ anions exhibit somewhat too long bonds compared to available experimental solid-state structures (cf., e.g., ref 37, see also ref 34 for a discussion of structures). To test the influence of these structural differences on the EPR parameters, we have also carried out a few BP86 calculations for the experimental structures. Changes for HFCs compared to results for optimized structures (cf. Table 2) were below 1.6 MHz for A_{iso} and below 0.3 MHz for T_{dip} for both complexes. Larger differences (between approximately 3000 and 10000 ppm) were obtained for the *g*-values with results for optimized structures generally in somewhat better agreement with experiment. We will in any case focus on DFT-optimized structures in the following since any future computations for systems of unknown structure will also have to employ structure optimizations.

Use of Pseudopotentials for *g*-Tensor Calculations. While the bulk of calculations in this work relied on an all-electron treatment that neglected scalar relativistic effects, we have also performed a few calculations (BP86 level) on $[MoOCl_4]^-$ where the core shells of Mo had been replaced by a small-core scalar relativistic pseudopotential[78] (effective core potential (ECP)) in the SCF step (with a 6s5p3d valence basis[78]) and a corresponding spin−orbit ECP[78] was used in the perturbational calculation of the SO matrix elements (eq 1).[28] The resulting $\Delta g_\perp = -42\,409$ ppm and $\Delta g_{||} = 3687$ ppm differ by 3000−4000 ppm from the all-electron results (Table 2), possibly in part as a consequence of scalar relativistic effects. In any case these results indicate that ECP/SO-ECP calculations may be of useful accuracy at very limited computational cost, for example, if one is not interested in the metal hyperfine couplings but only in *g*-tensors or ligand HFC tensors for Mo systems.

Two-Component *g*-Tensor Calculations. It has been noted previously that perturbational inclusion of spin−orbit coupling in a one-component second-order perturbation approach does not reproduce the negative parallel *g*-shifts ($\Delta g_{||}$) in heavy-atom Σ-radicals.[56,89] It appears thus reasonable to assume that the insufficiently negative $\Delta g_{||}$ components for $[MoOCl_4]^-$ and $[MoOF_5]^{2-}$ are also due to the neglect of higher-order SO

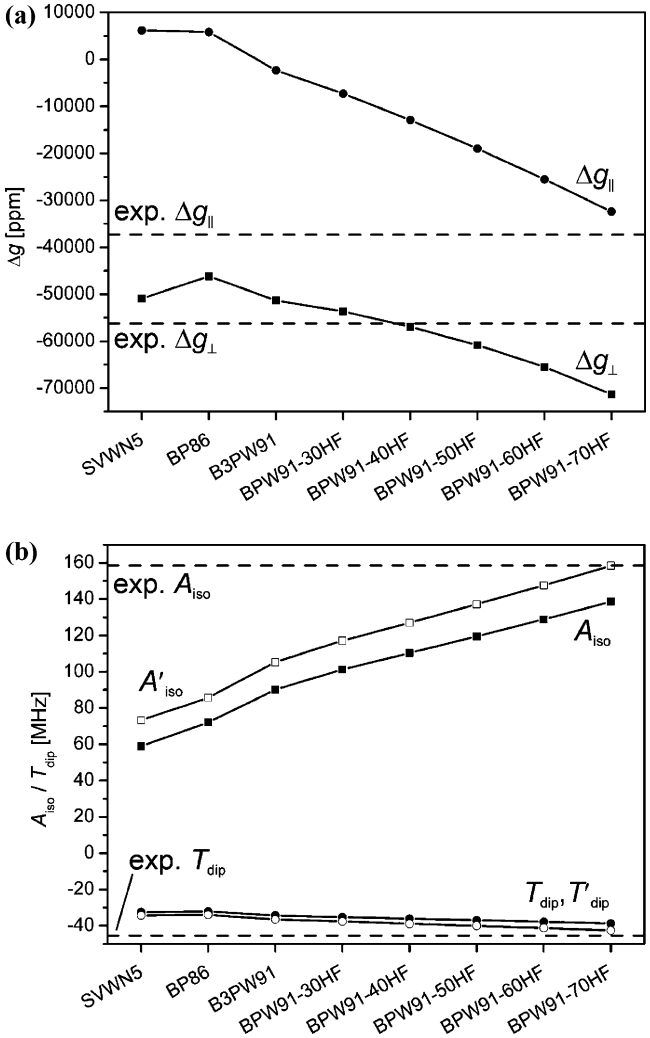

Figure 4. Dependence of (a) $\Delta g_\perp$ (squares) and $\Delta g_{||}$ (circles) and (b) ^{95}Mo A_{iso} (squares) and T_{dip} (circles), both with (open symbols) and without (closed symbols) SO-HFC corrections, on the choice of the density functional for $[MoOCl_4]^-$ ($^2B_2$). The calculations were performed using the 12s6p5d basis set for molybdenum and IGLO-II basis sets for all other atoms. The dashed lines indicate the experimental values[83] for (a) $\Delta g_\perp$ and $\Delta g_{||}$ as well as (b) A_{iso} and T_{dip}.

TABLE 3: Scalar Relativistic Effects on Mo HFC Tensors for $[MoOCl_4]^-$ ($^2B_2$) and $[MoOF_5]^{2-}$ ($^2B_2$)[a]

complex	method	A_{iso}	T_{dip}
$[MoOCl_4]^-$	BP86 NR[b]	67.3	−32.5
	BP86 DKH PN[c]	81.7	−32.0
	BP86 DKH FN[d]	80.0	−32.0
	B3PW91 NR[b]	84.7	−34.6
	B3PW91 DKH PN[c]	104.3	−33.8
	B3PW91 DKH FN[d]	100.9	−33.8
$[MoOF_5]^{2-}$	BP86 NR[b]	82.7	−35.9
	BP86 DKH PN[c]	111.8	−36.2
	BP86 DKH FN[d]	110.0	−36.2
	B3PW91 NR[b]	109.0	−38.3
	B3PW91 DKH PN[c]	137.3	−37.5
	B3PW91 DKH FN[d]	134.3	−37.5

[a] All computations were performed using the fully uncontracted Hirao 23s19p12d basis set for molybdenum and fully uncontracted DZVP basis sets for all other atoms. [b] Nonrelativistic calculation. [c] Relativistic second-order Douglas−Kroll−Hess calculation with point-nucleus model for both wavefunction and HFC operator. [d] Relativistic second-order Douglas−Kroll−Hess calculation with Gaussian finite-nucleus model for both wavefunction and HFC operator.

contributions. In addition to the second-order perturbation calculations presented, we have therefore also applied a recent relativistic non-collinear two-component DKH approach[56] to these two complexes at the BP86, B3PW91, BPW91-30HF, and BPW91-40HF levels. The results are included in Table 2 (values in parentheses).

While changes in $\Delta g_\perp$ compared to the one-component results at the corresponding DFT levels are moderate, the more negative $\Delta g_{||}$ values are notable for both complexes and with all functionals used. (The differences between one- and two-component results exhibit relatively little dependence on the functional.) Interestingly, the decrease of $\Delta g_{||}$ due to higher-order SO effects is larger for $[MoOF_5]^{2-}$ than for $[MoOCl_4]^-$ (ca. −20 vs ca. −11 ppt) whereas the decrease of $\Delta g_\perp$ is less pronounced (ca. −2 vs ca. −5 ppt). In both cases, the computed two-component $\Delta g_{||}$ values are appreciably closer to experiment than the one-component results. The deviations from experiment for a given functional have still not become identical for both tensor components. However, we note that the BPW91-30HF and BPW91-40HF levels do now provide the correct order $g_{||} < g_\perp$ for $[MoOF_5]^{2-}$.

As the two-component calculations in their current implementation are rather demanding for wider application to the larger systems discussed below and in the second paper of our validation study,[49] it appears most practical at this point to apply appropriate corrections for higher-order SO effects to the parallel ($\Delta g_{||}$ or Δg_{11}) components obtained in one-component second-order calculations. This should enhance the predictive power of the one-component approaches for large complexes.

Evaluation of Scalar Relativistic Effects on Mo Hyperfine Tensors by Second-Order DKH Calculations. When evaluating scalar relativistic effects on the Mo hyperfine couplings, we rely on an all-electron relativistic treatment: Table 3 compares nonrelativistic (NR) calculations of Mo hyperfine tensors with scalar relativistic calculations at the second-order DKH level with point-nucleus (PN) and finite-nucleus (FN) models, respectively,[71,72] using either the BP86 GGA or the B3PW91 hybrid functional. It is immediately obvious that relativistic effects (and effects of the nature of the nuclear model) are very small for the hyperfine anisotropies but are significant for the isotropic hyperfine couplings. For both systems and with both functionals, A_{iso} is enhanced appreciably, by ca. 19% for $[MoOCl_4]^-$ and by more than 20% for $[MoOF_5]^{2-}$. (In agreement with previous results,[72] compared to results with a finite-nucleus model, the point-nucleus calculations tend to overshoot somewhat the scalar relativistic effects on A_{iso}.)

We think that the relativistic enhancement factors obtained will be reasonably transferable to larger systems and may serve at least as good semiquantitative a posteriori correction factors on top of nonrelativistic calculations for larger systems. This should be kept in mind when evaluating the performance of different exchange−correlation functionals for isotropic hyperfine couplings below and in future studies.

EPR Parameters of $MoOLCl_2$ and $MoSLCl_2$ (L = Tris-(3,5-dimethylpyrazolyl)hydroborate). These two larger complexes (cf. Figure 1) provide us with a more challenging test of the methodology due to their lower symmetry. The latter point renders the orientations of the *g*- and HFC tensors nontrivial. Since very reliable single-crystal EPR studies are available for these systems,[76] we may evaluate the performance of DFT methods for tensor orientations relative to each other and to the molecular framework. We note that only very few single-crystal EPR studies of Mo^V compounds are available[6,41,76,82,86,90−93] due to the lack of suitable diamagnetic host lattices. This leads to a limited amount of experimental data on the orientation of the *g*- and HFC tensors relative to the molecular frame. For the $MoOLCl_2$ and $MoSLCl_2$ complexes, single-crystal Q-band EPR data are available,[76] and we may use them as "reference" systems before applying the computational methodology to an extended set of larger systems in a companion paper.[49] We note that a second single-crystal EPR study of $MoOLCl_2$[86] reports rather similar EPR parameters.

Figures 5 and 6 help to relate EPR parameters to bonding by visualizing the shape of the SOMO and the spin-density distribution, respectively, for both $MoXLCl_2$ complexes and for the GGA BP86 and the hybrid BPW91-40HF functionals. The SOMO (Figure 5) is mainly a molybdenum $4d_{xy}$ orbital with additional p-type contributions from the chlorine atoms (and to a lesser extent from the equatorial nitrogen ligands), and it possesses some metal−ligand π-antibonding character. (While the π-antibonding character relative to the axial ligand is obviously small for X = O, it can be seen for X = S upon inclusion of 40% HF exchange.)

The shape of the SOMO is roughly reflected in the positive part of the overall spin density (Figure 6). Additionally, however, negative spin density due to spin polarization is apparent at the axial ligand. Such negative spin density has recently been analyzed in detail by electron spin echo envelope modulation and DFT studies of oxygen HFC and NQC tensors in ^{17}O-labeled $[MoO(SPh)_4]^-$.[48] The negative spin density reflects the π-antibonding nature of the SOMO regarding the axial Mo−X bond. As has been discussed previously for 3d-complexes,[30] valence-shell spin polarization in transition-metal systems is closely related to metal−ligand σ- or π-antibonding character of the SOMO. It leads particularly to the polarization of the corresponding bonding doubly occupied MOs. The spin polarization differs notably for the two systems, in particular with respect to the dependence on the functional. While the negative spin density at the oxo ligand in $MoOLCl_2$ is increased moderately upon going from the BP86 GGA functional to the BPW91-40HF functional, the admixture of 40% HF exchange has a much more dramatic effect for $MoSLCl_2$. Whereas little negative spin density has developed at the axial sulfur ligand at the BP86 level, it is very pronounced in the BPW91-40HF calculations (Figure 6). Such a large dependence of valence-shell spin polarization on exact-exchange admixture has previ-

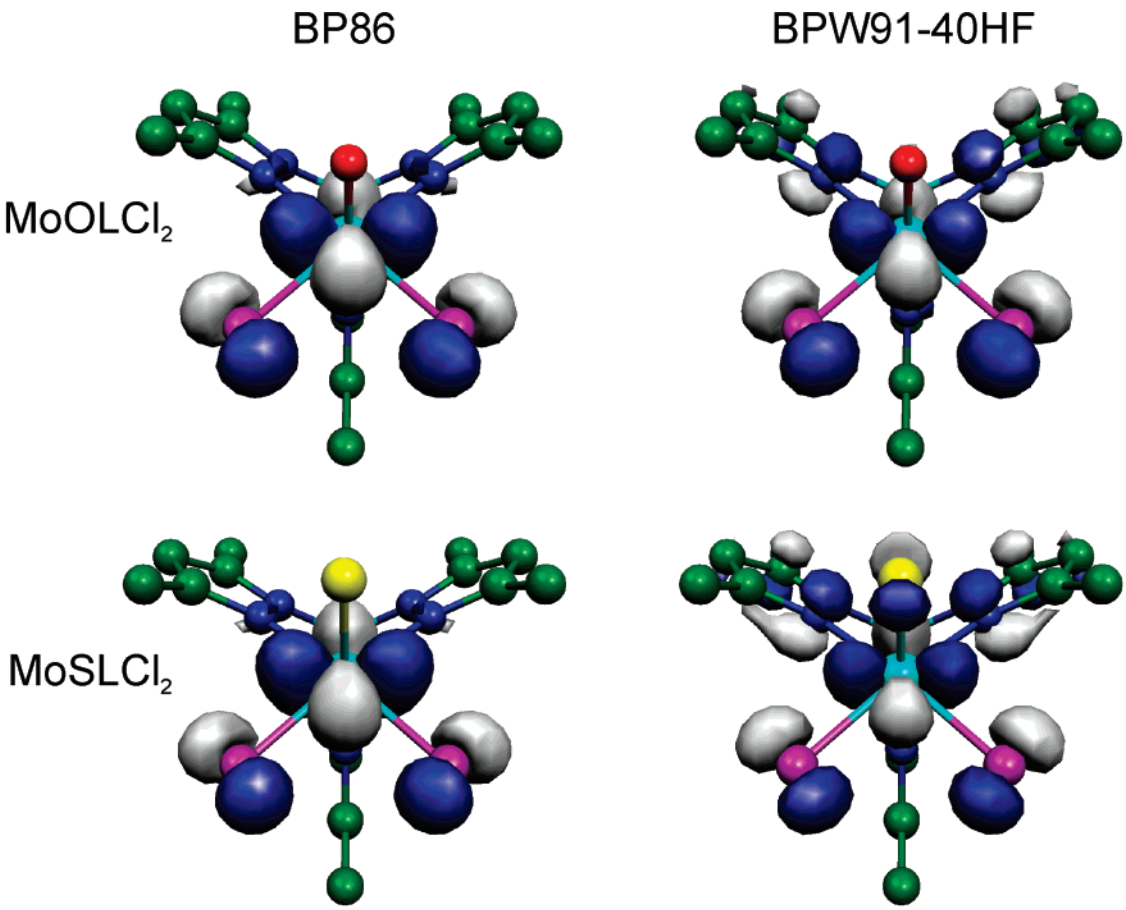

Figure 5. Isosurface plots of the SOMO (+/−0.05 a.u.) for $MoOLCl_2$ and $MoSLCl_2$ as calculated with BP86 or BPW91-40HF functionals, the 12s6p5d basis set for molybdenum, and IGLO-II basis sets for all other atoms. Positive amplitudes are shown in gray, and negative amplitudes in blue. Hydrogen atoms are omitted for the sake of clarity.

TABLE 4: Dependence of *g*-Tensor Principal Values on the Choice of the Density Functional for $MoOLCl_2$ and $MoSLCl_2$[a]

complex	functional	g_{11}	g_{22}	g_{33}	Δg_{11}	Δg_{22}	Δg_{33}	$\Delta g_{11} - \Delta g_{33}$[b]	$\Delta g_{11} - \Delta g_{22}/\Delta g_{11} - \Delta g_{33}$[c]	$\langle S^2 \rangle$
$MoOLCl_2$	SVWN5	2.0046	1.9423	1.9314	2290	−60051	−70957	73	0.85	0.7534
	BP86	2.0037	1.9483	1.9384	1351	−53982	−63934	65	0.85	0.7546
	B3PW91	1.9948	1.9427	1.9309	−7493	−59572	−71466	64	0.81	0.7601
	BPW91-30HF	1.9892	1.9404	1.9281	−13105	−61874	−74234	61	0.80	0.7661
	BPW91-40HF	1.9828	1.9370	1.9242	−19535	−65323	−78081	59	0.78	0.7754
	exp.[76]	1.969(1)	1.939(1)	1.931(1)	−33319	−63319	−71319	38	0.79	
$MoSLCl_2$	SVWN5	1.9987	1.9111	1.8839	−3616	−91224	−118419	115	0.76	0.7501
	BP86	1.9976	1.9244	1.9022	−4747	−77956	−100112	95	0.77	0.7643
	B3PW91	1.9860	1.9187	1.8972	−16345	−83627	−105168	89	0.76	0.8024
	BPW91-30HF	1.9780	1.9149	1.8962	−24298	−87443	−106128	82	0.77	0.8721
	BPW91-40HF	1.9685	1.9074	1.8921	−33795	−94935	−110193	76	0.80	0.9995
	exp.[76]	1.958(1)	1.911(1)	1.900(1)	−44319	−91319	−102319	58	0.81	

[a] All computations were performed using the 12s6p5d basis set for molybdenum and IGLO-II basis sets for all other atoms. The *g*-shifts (Δg) are given in ppm, and the *g*-anisotropy is given in ppt. The error of the experimental *g*-shifts is ±1000 ppm for both compounds. [b] *g*-Anisotropy $= \Delta g_{11} - \Delta g_{33}$ in ppt. [c] *g*-Tensor rhombicity $= (\Delta g_{11} - \Delta g_{22})/(\Delta g_{11} - \Delta g_{33})$.

ously been found to be connected to spin contamination with hybrid functionals[30] (see discussion below). This behavior is consistent[39] with a larger covalent nature of the Mo−S compared to the Mo−O multiple bond to the axial ligands. We may furthermore conclude from the shape of the SOMO that its s-character is negligible (Figure 5). We thus expect core−shell spin polarization to dominate the isotropic metal HFC values,[30,85] whereas the anisotropic parts will mainly be due to contributions from the unpaired electron in the SOMO.

We will use the "optimum" 12s6p5d molybdenum basis and focus on the comparison of different functionals and on the importance of spin−orbit corrections to the HFC tensors. *g*-Tensors are provided in Table 4, and HFC tensors in Table 5. Starting with the *g*-tensors, we see a similar behavior as for the smaller models above: Hybrid functionals with about 30−40% HF exchange admixture provide good agreement with experiment for the "perpendicular" components (Δg_{22} and Δg_{33}) but insufficiently negative "parallel" Δg_{11}-values. As we have seen above, the latter point is due to the neglect of higher-order spin−orbit contributions in the perturbational treatment. Therefore, the *g*-tensor anisotropy tends to be overestimated by the calculations (this could be improved at the two-component level, see above), while the rhombicity of the tensors is reproduced reasonably well. This is an observation that may bear on the comparison of theory and experiment for 4d-complexes on a more general level.

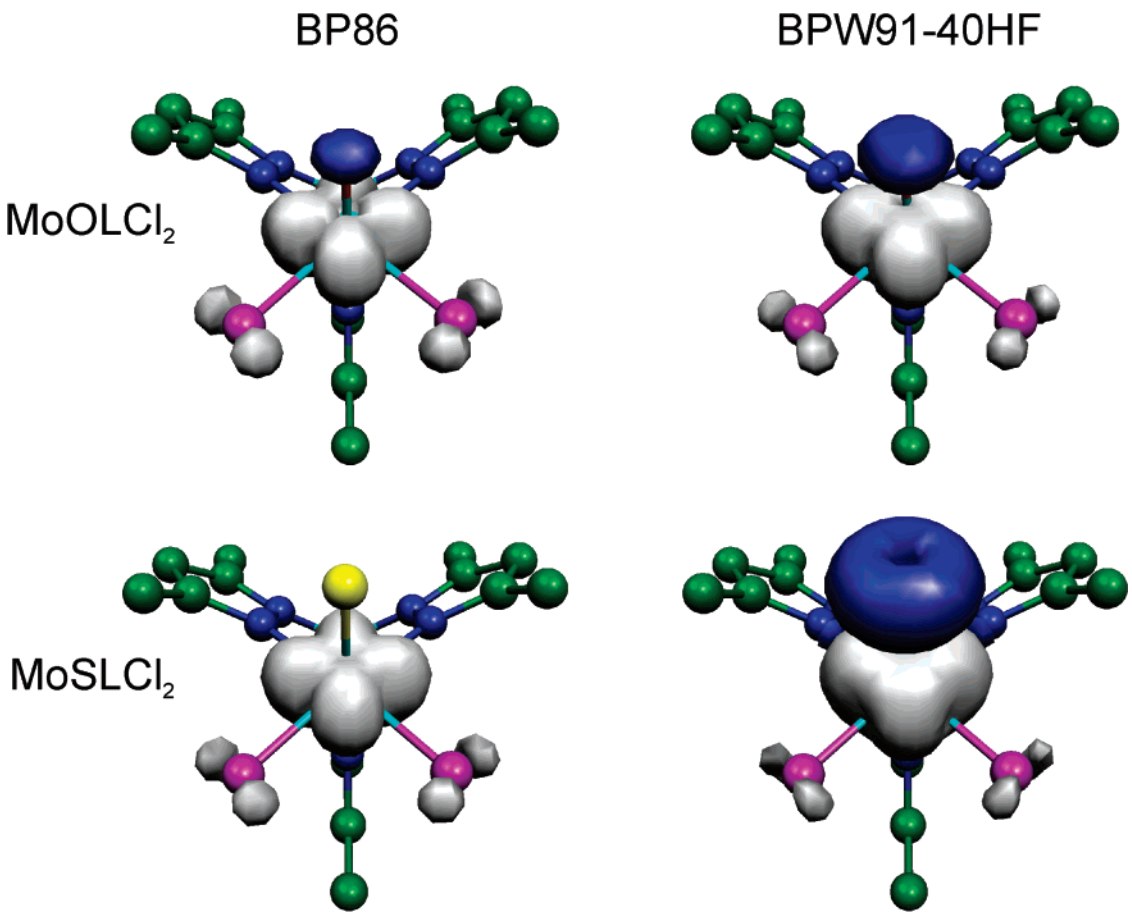

Figure 6. Isosurface plots of the spin-density distributions (+/−0.005 a.u.) for $MoOLCl_2$ and $MoSLCl_2$ as calculated with BP86 or BPW91-40HF functionals, the 12s6p5d basis set for molybdenum, and IGLO-II basis sets for all other atoms. Positive densities are shown in gray, and negative densities in blue. Hydrogen atoms are omitted for the sake of clarity.

TABLE 5: Dependence of HFC Constants on the Choice of the Density Functional for $MoOLCl_2$ and $MoSLCl_2$[a]

complex	functional	A_{FC}	A_{PC}	A'_{iso} [b]	T_{11}	T_{22}	T_{33}	$T_{11,orb}$	$T_{22,orb}$	$T_{33,orb}$	T'_{11} [c]	T'_{22} [c]	T'_{33} [c]	$\langle S^2 \rangle$
$MoOLCl_2$	SVWN5	56.5	14.7	71.3	60.3	−30.8	−29.5	5.6	−3.5	−2.0	64.3	−32.8	−31.5	0.7534
	BP86	69.9	14.0	83.9	59.9	−30.5	−29.4	5.4	−3.3	−2.1	64.1	−32.6	−31.5	0.7546
	B3PW91	89.5	15.9	105.5	64.4	−32.8	−31.7	6.5	−3.8	−2.8	69.9	−35.5	−34.4	0.7601
	BPW91-30HF	101.9	16.0	117.9	65.7	−33.4	−32.3	7.1	−3.9	−3.2	72.1	−36.6	−35.4	0.7661
	BPW91-40HF	112.6	17.9	130.4	67.0	−34.1	−32.9	7.7	−4.1	−3.6	73.9	−37.6	−36.3	0.7754
	exp.[76]			138(1)							77(2)	−38(2)	−37(2)	
$MoSLCl_2$	SVWN5	56.9	18.9	75.7	58.3	−29.9	−28.3	6.0	−5.0	−0.9	60.1	−30.8	−29.3	0.7501
	BP86	71.1	17.2	88.3	57.2	−29.3	−27.9	5.4	−4.2	−1.3	59.9	−30.5	−29.4	0.7643
	B3PW91	95.1	19.6	114.7	58.4	−30.0	−28.4	5.7	−3.7	−2.0	62.1	−32.0	−30.1	0.8024
	BPW91-30HF	113.7	21.0	134.7	56.1	−28.9	−27.3	5.6	−3.1	−2.5	60.4	−31.3	−29.1	0.8721
	BPW91-40HF	132.7	22.9	155.6	52.8	−26.8	−25.9	5.7	−3.1	−2.5	57.9	−30.0	−27.9	0.9995
	exp.[76]			140(1)							69(2)	−39(2)	−29(2)	

[a] First-order HFC constants (A_{FC} and T_{ii}), second-order SO correction terms (A_{PC} and $T_{ii,orb}$), as well as the total HFCs (A'_{iso} and T'_{ii}) are shown. The T_{ii}, $T_{ii,orb}$, and T'_{ii} values are given as eigenvalues of the corresponding tensors, i.e., in their own principal axis systems. All computations were performed using the 12s6p5d basis set for molybdenum and IGLO-II basis sets for all other atoms. All HFC constants are given in MHz. [b] $A'_{iso} = A_{FC} + A_{PC}$. [c] $T'_{ii} = T_{ii} + T_{ii,orb}$. This sum relation is only valid if the principal axis systems of all three tensors coincide. Since this is not the case for less symmetrical compounds, T'_{ii} will in general deviate from the sum of the two eigenvalues T_{ii} and $T_{ii,orb}$. The size of this deviation is an indicator of how much the axis systems differ from each other.

Turning to the HFC tensors (Table 5) and recalling that enhancement of A_{FC} by approximately 15−20% due to scalar relativistic effects is expected (cf. Table 3), we find good agreement with experimental isotropic couplings at approximately 30% HF exchange admixture. (This ratio appears to provide a reasonable description of core−shell spin polarization.) While the T_{ii} (T'_{ii}) parameters increase toward experiment with increasing HF exchange for $MoOLCl_2$, the situation is somewhat more complicated for $MoSLCl_2$: While the hyperfine anisotropy increases from the BP86 GGA functional to the B3PW91 hybrid functional, it decreases somewhat upon further increase of the HF exchange contribution. Such a behavior of the hyperfine anisotropy has been found to reflect nonnegligible spin contamination of the Kohn−Sham determinant in previous studies of hyperfine tensors for 3d transition metal complexes.[29,30] And indeed the $MoSLCl_2$ system is the only Mo^V complex in this study (and in our subsequent evaluation of a larger set of Mo^V complexes[49]) where the S^2 expectation value exhibits appreciable spin contamination upon increasing the HF exchange admixture beyond 20% (Table 5). In recent studies of *g*-tensors and spin-

TABLE 6: Relative Orientations of *g*- and HFC Tensors for $MoOLCl_2$ and $MoSLCl_2$ Expressed in Terms of the Angles between the Axes of the *g* and *A* Principal Axis Systems[a]

complex		computed orientation			experimental orientation[76]		
		A_{11}	A_{22}	A_{33}	A_{11}	A_{22}	A_{33}
$MoOLCl_2$							
	g_{11}	29.8	90.8	60.2	34.1	90.0	55.9
BP86	g_{22}	89.4	0.8	89.5	90.0	0.0	90.0
	g_{33}	119.8	90.2	29.8	124.1	90.0	34.1
		$\alpha = 1.1$	$\beta = 29.8$	$\gamma = -0.4$	$\alpha = 0$	$\beta = 34.1$	$\gamma = 0$
	g_{11}	31.0	90.7	59.1			
B3PW91	g_{22}	89.5	0.8	89.3			
	g_{33}	121.0	90.3	31.0			
		$\alpha = 1.3$	$\beta = 31.0$	$\gamma = -0.7$			
	g_{11}	32.7	91.6	57.3			
+SO-HFC correction	g_{22}	89.5	2.2	87.8			
	g_{33}	122.7	91.6	32.7			
		$\alpha = 4.1$	$\beta = 32.7$	$\gamma = -2.9$			
	g_{11}	31.6	90.7	58.4			
BPW91-30HF	g_{22}	89.6	0.7	89.4			
	g_{33}	121.6	90.3	31.6			
		$\alpha = 1.2$	$\beta = 31.6$	$\gamma = -0.6$			
	g_{11}	33.2	91.4	56.9			
+SO-HFC correction	g_{22}	89.6	1.9	88.2			
	g_{33}	123.2	91.3	33.2			
		$\alpha = 3.4$	$\beta = 33.2$	$\gamma = -2.4$			
	g_{11}	32.3	90.6	57.7			
BPW91-40HF	g_{22}	89.7	0.6	89.5			
	g_{33}	122.3	90.3	32.3			
		$\alpha = 1.0$	$\beta = 32.3$	$\gamma = -0.5$			
	g_{11}	33.8	91.1	56.2			
+SO-HFC correction	g_{22}	89.6	1.5	88.5			
	g_{33}	123.8	91.0	33.9			
		$\alpha = 2.7$	$\beta = 33.9$	$\gamma = -1.9$			
$MoSLCl_2$							
	g_{11}	32.2	90.1	57.8	30.7	90.0	59.3
BP86	g_{22}	90.1	0.5	89.5	90.0	0.0	90.0
	g_{33}	122.2	90.5	32.2	120.7	90.0	30.7
		$\alpha = 0.9$	$\beta = 32.2$	$\gamma = -0.9$	$\alpha = 0$	$\beta = 30.7$	$\gamma = 0$
	g_{11}	30.7	90.3	59.3			
B3PW91	g_{22}	90.1	0.6	89.4			
	g_{33}	120.7	90.5	30.7			
		$\alpha = 1.2$	$\beta = 30.7$	$\gamma = -1.1$			
	g_{11}	33.1	90.3	56.9			
+SO-HFC correction	g_{22}	90.0	0.6	89.4			
	g_{33}	123.1	90.5	33.1			
		$\alpha = 1.0$	$\beta = 33.1$	$\gamma = -0.9$			
	g_{11}	28.2	90.5	61.8			
BPW91-30HF	g_{22}	90.0	0.9	89.1			
	g_{33}	118.2	90.8	28.2			
		$\alpha = 1.9$	$\beta = 28.2$	$\gamma = -1.6$			
	g_{11}	30.2	90.5	59.8			
+SO-HFC correction	g_{22}	89.9	0.9	89.1			
	g_{33}	120.2	90.7	30.2			
		$\alpha = 1.7$	$\beta = 30.2$	$\gamma = -1.5$			
	g_{11}	24.0	91.2	66.0			
BPW91-40HF	g_{22}	89.8	2.6	87.4			
	g_{33}	114.0	92.3	24.1			
		$\alpha = 6.3$	$\beta = 24.1$	$\gamma = -5.5$			
	g_{11}	31.0	91.0	59.0			
+SO-HFC correction	g_{22}	90.0	2.0	88.0			
	g_{33}	121.0	91.8	31.0			
		$\alpha = 4.0$	$\beta = 31.0$	$\gamma = -3.4$			

[a] The eigenvectors of the two tensors are taken to span right-handed coordinate systems with an orientation of the axes in the molecular frame as shown exemplarily in Figure 7. Additionally, the corresponding Euler angles (defined as subsequent rotations around $z-y'-z''$ axes) are given. All computations were performed using the 12s6p5d basis set for molybdenum and IGLO-II basis sets for all other atoms. All angles are given in degrees.

density distributions of Ru^{III} $4d^5$ complexes with *ortho*-quinonoid ligands, we found a similar sensitivity of $\langle S^2 \rangle$ to exact-exchange admixture when one of the ligating atoms was sulfur, whereas no problems arose with oxygen. Closer analysis indicated that the larger covalency of the M−S bond gave rise to appreciable spin polarization of certain valence MOs, which was then overestimated at a higher fraction of HF exchange admixture.[39] The same effect is operative here (see discussion above).

Table 5 shows furthermore that SO contributions to the HFC tensors are of similar magnitude as found above for the smaller model complexes. That is, the SO contributions to A'_{iso} are

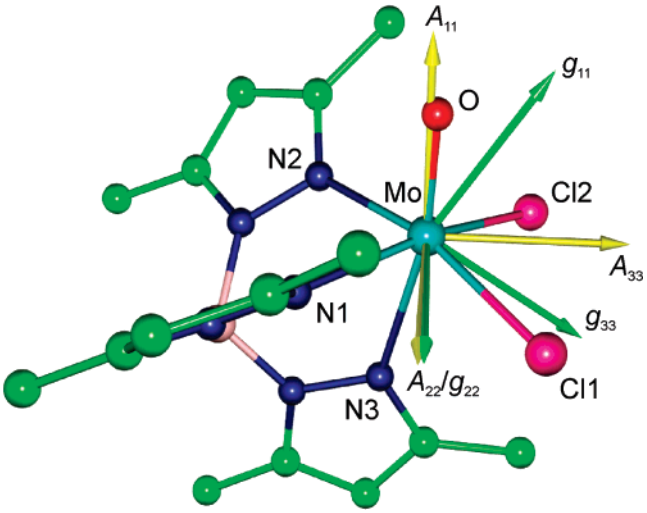

Figure 7. Computed orientation of the *g*- (green) and HFC (yellow, including SO corrections to the tensor orientation) tensors in the molecular frame for $MoOLCl_2$ (BPW91-40HF results). Principal axis systems are taken to be right-handed coordinate systems. For the sake of clarity all hydrogen atoms are omitted.

approximately 15−25% (the lower values hold for hybrid functionals, as the A_{PC} contribution increases less with HF exchange admixture than the nonrelativistic A_{FC} value), and those to T'_{dip} approximately 10%. In both cases, the absolute values are increased by the SO contributions and thus tend to move closer to the experimental data. It is clear that these second-order contributions should be included in accurate calculations.

Table 6 contains the computed and experimental[76] relative *g*- and *A*-tensor orientations for the two complexes. (Table S2 in the Supporting Information compares the tensor orientations relative to the molecular frame.) Figure 7 visualizes the computed tensor orientations for $MoOLCl_2$. The A_{11} axis points along the Mo−O bond, the A_{33} axis lies between the two chlorine atoms, and the A_{22} axis lies between a chlorine and an equatorial nitrogen atom. The g_{22} axis is almost collinear with A_{22}, and g_{11} and g_{33} are simply rotated clockwise around the g_{22}/A_{22} axis with respect to the principal axes of the HFC tensor. (The tensor orientations for $MoSLCl_2$ are shown in Figure S4 in the Supporting Information.) The agreement of the angles between the axes of the *g*- and HFC tensor principal axis systems with experiment is in general very satisfying for both complexes (Table 6). The influence of the density functional (amount of HF exchange) is rather small for $MoOLCl_2$ where changes of $g_{11}-A_{11}$ and $g_{33}-A_{33}$ angles are below 3° and changes of the $g_{22}-A_{22}$ angle are negligible. Increased exact-exchange admixture improves the computed orientation somewhat. The SO correction to the HFC tensor changes the orientation almost negligibly: $g_{11}-A_{11}$ and $g_{33}-A_{33}$ angle alterations are below 2° and the $g_{22}-A_{22}$ angle increases slightly by approximately 1° (i.e., these two axes are no longer completely collinear). The smallest deviations from experiment are found for BPW91-30HF and BPW91-40HF (including SO corrections to the HFC tensor). They are below 5% for the large $g_{11}-A_{11}$ and $g_{33}-A_{33}$ angles (corresponding to the Euler angle β for collinearity of g_{22} and A_{22}). For $MoSLCl_2$ the influence of the functional is somewhat different compared to $MoOLCl_2$. Going from BP86 to B3PW91 improves the computed orientation slightly (changes are smaller than 2°), but use of BPW91-40HF drastically deteriorates the agreement with experiment yielding, for example, too small angles between g_{11} and A_{11} as well as g_{33} and A_{33} (cf. Table 6). This reflects probably the onset of substantial spin contamination above exact-exchange admixtures of 20% (see discussion above). Inclusion of SO corrections to the HFC tensor leads to very small alterations of the angles (e.g., below 3° for $g_{11}-A_{11}$ and $g_{33}-A_{33}$ angles) for B3PW91 but influences the HFC tensor orientation much more for BPW91-40HF (e.g., 7° for $g_{11}-A_{11}$ and $g_{33}-A_{33}$ angles). The spin-contamination problem thus shows itself also for the tensor orientations and makes the choice of an ideal functional more difficult for this particular complex. (As noted above, none of the larger variety of systems discussed in our second paper[49] exhibits such problems.) Probably the B3PW91 calculations (with SO corrections to the HFC tensor) would appear the most reliable approach in this case.

The orientation of *g*- and molybdenum HFC tensors in the molecular frame (Figure 7) is reproduced very well by the calculations (Table S2 in the Supporting Information) with the same influence of functional and SO corrections to HFC tensors as discussed for the relative tensor orientations. The angles between the principal tensor axes and the Mo−X bonds (X = O/S, Cl1, Cl2, N1, N2, N3) indicate deviations for the g_{11}/A_{11}, g_{22}/A_{22}, and g_{33}/A_{33} axes of 5°, 2°, and 4°, or better, for $MoOLCl_2$ and 6−7°, 2°, and 3−5°, or better for $MoSLCl_2$. The largest deviations are found for angles of the tensor axes with the Mo−O/S bond and the Mo−Cl bonds. These results support thus the predictive power of appropriate DFT methods for the relative and absolute tensor orientations. This is of importance when applying DFT methods to systems where the tensor orientations are less well-known from experiment.

4. Conclusions

This study suggests that in most cases both molybdenum hyperfine tensors and *g*-tensors of Mo^V systems are well reproduced by hybrid DFT methods with approximately 30−40% exact-exchange admixture. The following limitations have to be kept in mind, however: (a) The "parallel" *g*-tensor component comes out insufficiently negative in treatments that include spin−orbit coupling only to leading order in perturbation theory. Here, a variational inclusion of spin−orbit coupling becomes necessary, for example, in a two-component framework. (The non-collinear two-component DKH approach used in this work has the advantage of taking into account spin polarization.[56]) It appears possible that a more detailed understanding of the *g*-tensors may allow the systematic correction of one-component results for the missing higher-order SO contributions. (b) In certain, relatively rare cases (in the present paper only the $MoSLCl_2$ system), the onset of spin contamination may deteriorate the results for large exact-exchange admixtures. These cases may, however, be identified straightforwardly. (The problems are related to an appreciable metal−ligand antibonding nature of the singly occupied MOs.) Then use of a lower fraction of HF exchange (as, e.g., in the B3-type hybrid functionals) may still provide reasonably accurate EPR parameters. An alternative for such cases in future studies may be the use of localized hybrid potentials.[44,45] (c) Isotropic Mo hyperfine couplings (more precisely, their Fermi-contact-type part) tend to be enhanced by about 15−20% when scalar relativistic effects are taken into account. This has to be kept in mind when comparing nonrelativistic calculations to experiment.

Notably, the detailed comparison of theory and single-crystal experiments for two larger, less symmetrical $MoXLCl_2$ (X = O,S; L = tris(3,5-dimethylpyrazolyl)hydroborate anion) complexes indicates good predictive power of the chosen DFT approaches for relative and absolute orientations of *g*- and metal HFC tensors. Spin−orbit corrections to the molybdenum HFC tensor components are significant and should be included in

accurate calculations (but their influence on the tensor orientations was only moderate). Detailed basis-set calibration studies have provided us with a moderate-sized 12s6p5d basis set for molybdenum that provides an excellent compromise between accuracy for molybdenum hyperfine tensor calculations and computational effort.

Acknowledgment. J.F. and P.H. acknowledge financial support by the DFG (SFB 472 "Molecular Bioenergetics"). Work in Bratislava has also been supported by the Slovak Grant Agencies APVV (Grant No. 0625-06) and VEGA (Grant No. 2/6182/26). M.K. acknowledges financial support by DFG (project KA1187/4-2 within priority programme "High-Field EPR"), and Dr. R. Reviakine, Professor T. F. Prisner, and the Frankfurt Center for Scientific Computing are thanked for their technical support.

Supporting Information Available: Detailed analysis of MO contributions to the *g*-tensor for $[MoOCl_4]^-$ including isodensity surface plots of various MOs, figures displaying dependence of *g*-values on size of molybdenum basis set for Mo atom and MoN, figure and table describing the orientation of *g*- and HFC tensors with respect to the molecular frame for $MoXLCl_2$ complexes, and tables of Cartesian coordinates of all optimized structures (including *g*- and HFC tensor principal axis systems for the $MoXLCl_2$ compounds). This material is available free of charge via the Internet at http://pubs.acs.org.

References and Notes

(1) Hille, R. *Chem. Rev.* **1996**, *96*, 2757−2816.
(2) Hille, R. *Trends Biochem. Sci.* **2002**, *27*, 360−367.
(3) Enemark, J. H.; Cooney, J. J. A.; Wang, J.-J.; Holm, R. H. *Chem. Rev.* **2004**, *104*, 1175−1200.
(4) *Molybdenum and Tungsten: Their Roles in Biological Processes*; Sigel, A., Sigel, H., Eds.; Metal Ions in Biological Systems 39; Marcel Dekker: New York, 2002.
(5) Schweiger, A.; Jeschke, G. *Principles of Pulse Electron Paramagnetic Resonance*; Oxford University Press: Oxford, U. K., 2001.
(6) Mabbs, F. E.; Collison, D. *Electron Paramagnetic Resonance of d Transition Metal Compounds*; Elsevier Science: Amsterdam, 1992.
(7) Bray, R. C. *Q. Rev. Biophys.* **1988**, *21*, 299−329.
(8) Astashkin, A. V.; Feng, C.; Raitsimring, A. M.; Enemark, J. H. *J. Am. Chem. Soc.* **2005**, *127*, 502−503.
(9) Astashkin, A. V.; Hood, B. L.; Feng, C.; Hille, R.; Mendel, R. R.; Raitsimring, A. M.; Enemark, J. H. *Biochemistry* **2005**, *44*, 13274−13281.
(10) Gordy, W. *Theory and Applications of Electron Spin Resonance*; Techniques of Chemistry 15; John Wiley & Sons: New York, 1980.
(11) Prisner, T.; Lyubenova, S.; Atabay, Y.; MacMillan, F.; Kröger, A.; Klimmek, O. *J. Biol. Inorg. Chem.* **2003**, *8*, 419−426.
(12) Bennati, M.; Hertel, M. M.; Fritscher, J.; Prisner, T. F.; Weiden, N.; Hofweber, R.; Spoerner, M.; Horn, G.; Kalbitzer, H.-R. *Biochemistry* **2006**, *45*, 42−50.
(13) Schiemann, O.; Fritscher, J.; Kisseleva, N.; Sigurdsson, S. T.; Prisner, T. F. *ChemBiolChem* **2003**, *4*, 1057−1065.
(14) Bennati, M.; Prisner, T. F. *Rep. Prog. Phys.* **2005**, *68*, 411−448.
(15) Fritscher, J.; Artin, E.; Wnuk, S.; Bar, G.; Robblee, J. H.; Kacprzak, S.; Kaupp, M.; Griffin, R. G.; Bennati, M.; Stubbe, J. *J. Am. Chem. Soc.* **2005**, *127*, 7729−7738.
(16) Wertz, J. E.; Bolton, J. R. *Electron Spin Resonance: Elementary Theory and Practical Applications*; McGraw-Hill: New York, 1972.
(17) Bennati, M.; Robblee, J. H.; Mugnaini, V.; Stubbe, J.; Freed, J. H.; Borbat, P. *J. Am. Chem. Soc.* **2005**, *127*, 15014−15015.
(18) Kaupp, M.; Malkin, V. G.; Bühl, M., Eds. *Calculation of NMR and EPR Parameters*; Wiley-VCH: Weinheim, Germany, 2004.
(19) Fritscher, J. *Phys. Chem. Chem. Phys.* **2004**, *6*, 4950−4956.
(20) Parr, R. G.; Yang, W. *Density-Functional Theory of Atoms and Molecules*; Oxford University Press: New York, 1989.
(21) Schreckenbach, G.; Ziegler, T. *J. Phys. Chem. A* **1997**, *101*, 3388−3399.
(22) van Lenthe, E.; van der Avoird, A.; Wormer, P. E. S. *J. Chem. Phys.* **1998**, *108*, 4783−4796.
(23) Arratia-Perez, R.; Case, D. A. *J. Chem. Phys.* **1983**, *79*, 4939−4949.
(24) Patchkovskii, S.; Ziegler, T. *J. Am. Chem. Soc.* **2000**, *122*, 3506−3516.
(25) Neese, F. *J. Chem. Phys.* **2003**, *118*, 3939−3948.
(26) Neese, F. *J. Chem. Phys.* **2001**, *115*, 11080−11096.
(27) Malkina, O. L.; Vaara, J.; Schimmelpfennig, B.; Munzarová, M.; Malkin, V. G.; Kaupp, M. *J. Am. Chem. Soc.* **2000**, *122*, 9206−9218.
(28) Kaupp, M.; Reviakine, R.; Malkina, O. L.; Arbuznikov, A.; Schimmelpfennig, B.; Malkin, V. G. *J. Comput. Chem.* **2002**, *23*, 794−803.
(29) Munzarová, M.; Kaupp, M. *J. Phys. Chem. A* **1999**, *103*, 9966−9983.
(30) Munzarová, M. L.; Kubácek, P.; Kaupp, M. *J. Am. Chem. Soc.* **2000**, *122*, 11900−11913.
(31) Belanzoni, P.; Baerends, E. J.; van Asselt, S.; Langewen, P. B. *J. Phys. Chem.* **1995**, *99*, 13094−13102.
(32) Remenyi, C.; Reviakine, R.; Arbuznikov, A. V.; Vaara, J.; Kaupp, M. *J. Phys. Chem. A* **2004**, *108*, 5026−5033.
(33) Neese, F. *Curr. Opin. Chem. Biol.* **2003**, *7*, 125−135.
(34) Patchkovskii, S.; Ziegler, T. *J. Chem. Phys.* **1999**, *111*, 5730−5740.
(35) Sunil, K. K.; Harrison, J. F.; Rogers, M. T. *J. Chem. Phys.* **1982**, *76*, 3087−3097.
(36) Peng, G.; Nichols, J.; McCullough, E. A., Jr; Spence, J. T. *Inorg. Chem.* **1994**, *33*, 2857−2864.
(37) Swann, J.; Westmoreland, T. D. *Inorg. Chem.* **1997**, *36*, 5348−5357.
(38) Li, W.; Hong, M.; Cao, R.; Kang, B.; Liu, H. *J. Magn. Reson.* **1999**, *138*, 80−88.
(39) Remenyi, C.; Kaupp, M. *J. Am. Chem. Soc.* **2005**, *127*, 11399−11413.
(40) Remenyi, C.; Munzarová, M. L.; Kaupp, M. *J. Phys. Chem. B* **2005**, *109*, 4227−4233.
(41) Cosper, M. M.; Neese, F.; Astashkin, A. V.; Carducci, M. D.; Raitsimring, A. M.; Enemark, J. H. *Inorg. Chem.* **2005**, *44*, 1290−1301.
(42) Sinnecker, S.; Neese, F.; Noodleman, L.; Lubitz, W. *J. Am. Chem. Soc.* **2004**, *126*, 2613−2622.
(43) Frantz, S.; Hartmann, H.; Doslik, N.; Wanner, M.; Kaim, W.; Kümmerer, H.-J.; Denninger, G.; Barra, A.-L.; Duboc-Toia, C.; Fiedler, J.; Ciofini, I.; Urban, C.; Kaupp, M. *J. Am. Chem. Soc.* **2002**, *124*, 10563−10571.
(44) Arbuznikov, A. V.; Kaupp, M. *Chem. Phys. Lett.* **2004**, *391*, 16−21.
(45) Arbuznikov, A. V.; Kaupp, M. *Int. J. Quantum Chem.* **2005**, *104*, 261−271.
(46) Patchkovskii, S.; Ziegler, T. *J. Phys. Chem. A* **2001**, *105*, 5490−5497.
(47) Arbuznikov, A. V.; Kaupp, M.; Malkin, V. G.; Reviakine, R.; Malkina, O. L. *Phys. Chem. Chem. Phys.* **2002**, *4*, 5467−5474.
(48) Astashkin, A. V.; Neese, F.; Raitsimring, A. M.; Cooney, J. J. A.; Bultman, E.; Enemark, J. H. *J. Am. Chem. Soc.* **2005**, *127*, 16713−16722.
(49) Fritscher, J.; Hrobárik, P.; Kaupp, M. *Inorg. Chem.*, submitted for publication.
(50) Arbuznikov, A. V.; Vaara, J.; Kaupp, M. *J. Chem. Phys.* **2004**, *120*, 2127−2139.
(51) Malkin, V. G.; Malkina, O. L.; Reviakine, R.; Arbuznikov, A. V.; Kaupp, M.; Schimmelpfennig, B.; Malkin, I.; Helgaker, T.; Ruud, K., *MAG-ReSpect*, version 1.2; 2004.
(52) Abragam, A.; Bleaney, B. *Electron Paramagnetic Resonance of Transition Ions*; Oxford Clarendon Press: Oxford, U. K., 1970.
(53) Harriman, J. E. *Theoretical Foundations of Electron Spin Resonance*; Academic Press: New York, 1978.
(54) Weltner, W. *Magnetic Atoms and Molecules*; Dover Publications: New York, 1983.
(55) Moss, R. E. *Advanced Molecular Quantum Mechanics*; Chapman and Hall: London, 1973.
(56) Malkin, I.; Malkina, O. L.; Malkin, V. G.; Kaupp, M. *J. Chem. Phys.* **2005**, *123*, 244103.
(57) Frisch, M. J.; Trucks, G. W.; Schlegel, H. B.; Scuseria, G. E.; Robb, M. A.; Cheeseman, J. R.; Montgomery, J. A., Jr.; Vreven, T.; Kudin, K. N.; Burant, J. C.; Millam, J. M.; Iyengar, S. S.; Tomasi, J.; Barone, V.; Mennucci, B.; Cossi, M.; Scalmani, G.; Rega, N.; Petersson, G. A.; Nakatsuji, H.; Hada, M.; Ehara, M.; Toyota, K.; Fukuda, R.; Hasegawa, J.; Ishida, M.; Nakajima, T.; Honda, Y.; Kitao, O.; Nakai, H.; Klene, M.; Li, X.; Knox, J. E.; Hratchian, H. P.; Cross, J. B.; Bakken, V.; Adamo, C.; Jaramillo, J.; Gomperts, R.; Stratmann, R. E.; Yazyev, O.; Austin, A. J.; Cammi, R.; Pomelli, C.; Ochterski, J. W.; Ayala, P. Y.; Morokuma, K.; Voth, G. A.; Salvador, P.; Dannenberg, J. J.; Zakrzewski, V. G.; Dapprich, S.; Daniels, A. D.; Strain, M. C.; Farkas, O.; Malick, D. K.; Rabuck, A. D.; Raghavachari, K.; Foresman, J. B.; Ortiz, J. V.; Cui, Q.; Baboul, A. G.; Clifford, S.; Cioslowski, J.; Stefanov, B. B.; Liu, G.; Liashenko, A.; Piskorz, P.; Komaromi, I.; Martin, R. L.; Fox, D. J.; Keith, T.; Al-Laham, M. A.; Peng, C. Y.; Nanayakkara, A.; Challacombe, M.; Gill, P. M. W.; Johnson, B.; Chen, W.; Wong, M. W.; Gonzalez, C.; Pople, J. A. *Gaussian 03*, revision C.02; Gaussian, Inc.: Wallingford, CT, 2004.

(58) Vosko, S. H.; Wilk, L.; Nusair, M. *Can. J. Phys.* **1980**, *58*, 1200−1211.
(59) Becke, A. D. *Phys. Rev. A* **1988**, *38*, 3098−3100.
(60) Perdew, J. P.; Wang, Y. *Phys. Rev. B* **1986**, *33*, 8822−8824.
(61) Perdew, J. P.; Wang, Y. *Phys. Rev. B* **1986**, *34*, 7406.
(62) Becke, A. D. *J. Chem. Phys.* **1993**, *98*, 1372−1377.
(63) Becke, A. D. *J. Chem. Phys.* **1993**, *98*, 5648−5652.
(64) Perdew, J. P. *Physica B* **1991**, *172*, 1−6.
(65) Perdew, J. P.; Wang, Y. *Phys. Rev. B* **1992**, *45*, 13244−13249.
(66) Hess, B. A.; Marian, C. M.; Wahlgren, U.; Gropen, O. *Chem. Phys. Lett.* **1996**, *251*, 365−371.
(67) Schimmelpfennig, B. *AMFI, Atomic Spin−Orbit Mean-Field Integral Program*; Stockholms Universitet: Stockholm, Sweden, 1996.
(68) Ahlrichs, R.; May, K. *Phys. Chem. Chem. Phys.* **2000**, *2*, 943−945.
(69) Tsuchiya, T.; Abe, M.; Nakajima, T.; Hirao, K. *J. Chem. Phys.* **2001**, *115*, 4463−4472.
(70) Kutzelnigg, W.; Fleischer, U.; Schindler, M. In *NMR Basic Principles and Progress*; Diehl, P., Fluck, E., Günther, H., Kosfeld, R., Seelig, J., Eds.; Springer-Verlag: Berlin/Heidelberg, 1991; Vol. 23, pp 165−262.
(71) Malkin, I.; Malkina, O. L.; Malkin, V. G.; Kaupp, M. *Chem. Phys. Lett.* **2004**, *396*, 268−276.
(72) Malkin, E.; Malkin, I.; Malkina, O. L.; Malkin, V. G.; Kaupp, M. *Phys. Chem. Chem. Phys.* **2006**, 4079−4085.
(73) Godbout, N.; Salahub, D. R.; Andzelm, J.; Wimmer, E. *Can. J. Chem.* **1992**, *70*, 560−571.
(74) Knight, L. B., Jr.; Steadman, J. *J. Chem. Phys.* **1982**, *76*, 3378−3384.
(75) Shim, I.; Gingerich, K. A. *J. Mol. Struct. (THEOCHEM)* **1999**, *460*, 123−136.
(76) Collison, D.; Eardley, D. R.; Mabbs, F. E.; Rigby, K.; Bruck, M. A.; Enemark, J. H.; Wexler, P. A. *J. Chem. Soc., Dalton Trans.* **1994**, 1003−1011.
(77) Ahlrichs, R.; Bär, M.; Baron, H.; Bauernschmitt, R.; Böcker, S.; Deglmann, P.; Ehrig, M.; Eichkorn, K.; Elliott, S.; Furche, F.; Haase, F.; Häser, M.; Horn, H.; Hättig, C.; Huber, C.; Huniar, U.; Kattannek, M.; Köhn, A.; Kölmel, C.; Kollwitz, M.; May, K.; Ochsenfeld, C.; Öhm, H.; Schäfer, A.; Schneider, U.; Sierka, M.; Treutler, O.; Unterreiner, B.; von Arnim, M.; Weigend, F.; Weis, P.; Weiss, H. *Turbomole*, version 5.6; Quantum Chemistry Group, University of Karlsruhe: Karlsruhe, Germany, 2002.
(78) Andrae, D.; Häussermann, U.; Dolg, M.; Stoll, H.; Preuss, H. *Theor. Chim. Acta* **1990**, *77*, 123−141.
(79) Schäfer, A.; Huber, C.; Ahlrichs, R. *J. Chem. Phys.* **1994**, *100*, 5829−5835.
(80) Eichkorn, K.; Treutler, O.; Öhm, H.; Häser, M.; Ahlrichs, R. *Chem. Phys. Lett.* **1995**, *242*, 652−660.
(81) Eichkorn, K.; Weigend, F.; Treutler, O.; Ahlrichs, R. *Theor. Chem. Acc.* **1997**, *97*, 119−124.
(82) Balagopalakrishna, C.; Kimbrough, J. T.; Westmoreland, T. D. *Inorg. Chem.* **1996**, *35*, 7758−7768.
(83) Sunil, K. K.; Rogers, M. T. *Inorg. Chem.* **1981**, *20*, 3283−3287.
(84) Manoharan, P. T.; Rogers, M. T. *J. Chem. Phys.* **1968**, *49*, 5510−5519.
(85) Watson, R. E.; Freeman, A. J. In *Hyperfine Interactions*; Freeman, A. J.; Frankel, R. B., Eds.; Academic Press: New York, 1967, pp 53−94.
(86) Nipales, N. S.; Westmoreland, T. D. *Inorg. Chem.* **1997**, *36*, 756−757.
(87) Schreckenbach, G. *J. Chem. Phys.* **1999**, *110*, 11936−11949.
(88) Izumi, Y.; Glaser, T.; Rose, K.; McMaster, J.; Basu, P.; Enemark, J. H.; Hedman, B.; Hodgson, K. O.; Solomon, E. I. *J. Am. Chem. Soc.* **1999**, *121*, 10035−10046.
(89) Patchkovskii, S.; Schreckenbach, G. In *Calculation of NMR and EPR Parameters*; Kaupp, M., Malkin, V. G., Bühl, M., Eds.; Wiley-VCH: Weinheim, Germany, 2004; pp 505−532.
(90) Garner, C. D.; Hill, L. H.; Mabbs, F. E.; McFadden, D. L.; McPhail, A. T. *J. Chem. Soc., Dalton Trans.* **1977**, 853−858.
(91) Garner, C. D.; Lambert, P.; Mabbs, F. E.; King, T. J. *J. Chem. Soc., Dalton Trans.* **1977**, 1191−1198.
(92) Garner, C. D.; Howlander, N. C.; Mabbs, F. E.; Boorman, P. M.; King, T. J. *J. Chem. Soc., Dalton Trans.* **1978**, 1350−1354.
(93) Gahan, B.; Howlander, N. C.; Mabbs, F. E. *J. Chem. Soc., Dalton Trans.* **1981**, 142−149.